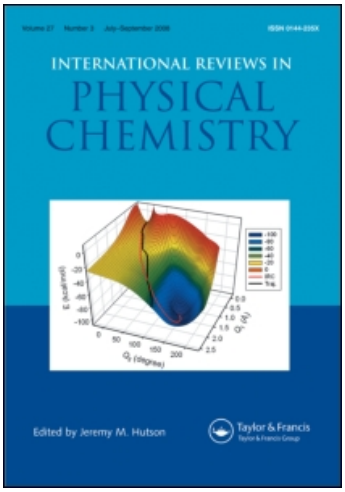

International Reviews in Physical Chemistry
Publication details, including instructions for authors and subscription information:
http://www.informaworld.com/smpp/title~content=t713724383

Compton Scattering as a Technique for the Study of Solids

B. G. Williams[a]; J. M. Thomas[a]
[a] Department of Physical Chemistry, University, of Cambridge, Cambridge, CB2 1EP

To cite this Article Williams, B. G. and Thomas, J. M.(1983) 'Compton Scattering as a Technique for the Study of Solids', International Reviews in Physical Chemistry, 3: 1, 39 — 82
To link to this Article: DOI: 10.1080/01442358309353339
URL: http://dx.doi.org/10.1080/01442358309353339

International Reviews in Physical Chemistry (1983), *3* (39–82)

COMPTON SCATTERING AS A TECHNIQUE FOR THE STUDY OF SOLIDS

B. G. WILLIAMS AND J. M. THOMAS

Department of Physical Chemistry, University, of Cambridge, Lensfield Road, Cambridge CB2 1EP, UK

ABSTRACT

Starting with an historical account of the emergence of the Compton effect, the review summarizes the essential features of the processes involved in Compton scattering and outlines the theory required to interpret Compton profiles in terms of the momentum density, momentum wavefunctions and position wavefunctions. In this connection the essentials of the impulse approximation and the convenient concept of the reciprocal form factor are explained. Experimental procedures for the determination of Compton profiles using γ-ray, X-ray and electron sources are briefly described and so also is positron annihilation. The advantages and insights afforded by Compton profile measurements in the study of electronic properties are illustrated by reference to a range of materials including elemental and several binary solids. Future prospects, especially in solid-state chemistry where Compton scattering could prove advantageous, are briefly outlined.

1. INTRODUCTION

General considerations

Chemists are often preoccupied with the establishment of atomic and electronic structure and they have a continuing interest in the development of new and the extension of old techniques for structural elucidation. In the last decade several important developments have been made in this connection, especially in the refinements that permit structures to be determined under circumstances where conventional techniques such as X-ray crystallography cannot be applied. Thus in the study of microcrystalline and amorphous materials and their surfaces, which generally lie beyond the scope of X-ray methods, much progress in deducing the nature of truly microscopic (atomic) structure has been accomplished by the application of techniques such as neutron scattering, extended-X-ray-absorption-fine-structure (EXAFS), X-ray-absorption-near-edge-structure (XANES), X-ray and u.v.-induced photoelectron spectroscopies (XPS and UPS), Bremstrahlung isochromat spectroscopy (BIS), high resolution electron microscopy (HREM), electron energy loss spectroscopy (EELS), magic-angle-spinning NMR (MASNMR) and high sensitivity nuclear quadrupole resonance using various kinds of double resonance methods (e.g., DRLC). The last three named techniques have been reviewed in earlier issues of this journal (*see* Rao *et al.*, 1981, on EELS; Andrew, 1981, on MASNMR; and Edmonds, 1982, on NQR). Here, we shall focus upon the scope and prospects of another, less-widely known technique, Compton scattering, which may be applied equally to the study of isolated

0144-235X/83/01 0039-40 $03.00

(gas phase) species as well as to condensed matter (liquids, amorphous materials and crystalline solids).

In recent years there has been a revival of interest in Compton scattering, partly because it is now relatively straightforward and inexpensive to conduct the appropriate experiments thanks to the availability of high-energy, high-intensity γ-ray and X-ray sources, synchrotrons, electron microscopes, energy dispersive detectors and multichannel analysers, but also because of a growing awareness of the important physicochemical information that the measurement of Compton profiles yields. We shall describe in subsequent sections how various important properties of a system may be extracted from measured Compton profiles. At this stage it is instructive to recall that, in Compton scattering experiments, we obtain information about the momenta of the electrons in the sample. To be precise one measures, in effect, the ground-state momentum density, $\rho(\boldsymbol{p})$, which is the square of the momentum wave function $\chi(\boldsymbol{p})$ and this in turn is the Fourier transform of the position wavefunction. Compton scattering therefore provides direct access to the electronic ground state wavefunction of the sample. In the final analysis, all the structural, chemical and other properties of a system are governed by the respective wavefunctions; it can therefore be appreciated that a technique which enables us to probe the momentum or position density directly is potentially very powerful.

Historical background

Although Compton scattering lies beyond the horizon of experience of most chemists, the Compton effect itself, in view of its prominence in university textbooks, is very familiar. Its discovery constituted an important landmark in the evolution of the quantum theory in that it offered compelling evidence for the notion of a photon or a quantum of light. A. H. Compton established (Compton, 1922, 1923a,b) that when X-rays are scattered by a solid target there is an increase in the wavelength of the X-ray. The scattered X-rays have intensity peaks at two wavelengths, one being essentially the same as the incident wavelength, λ, the other λ', being larger by an amount $\Delta\lambda$.* This so-called Compton shift varies with the angle at which the scattered X-rays are observed (ϕ in *Fig. 1*) but is independent of the chemical nature of the target and of the initial wavelength. Using the concept of light quantum momentum, $h\nu/c$, which had been introduced explicitly by Stark (1909, 1910), Compton showed that†

* It is interesting to note that two years before Compton's seminal paper Debye had carried out exactly the same calculation as an exercise in the application of Einstein's light quantum hypothesis but had refrained from publishing it because of the lack of experimental evidence. On reading a brief account by Compton of his experimental results Debye published his theory of the scattering of photons by free electrons (Debye, 1923), his paper appearing in print one month before Compton's paper (Compton, 1923a). As Compton had independently derived the theory and had also carried out the crucial experiments Debye graciously conceded that the effect should bear Compton's name alone.

† Eq. (1) may be derived by applying the conservation of energy and linear momentum to the situation depicted in *Figure 1*. Since the scattered (recoil) electron has a speed v comparable with the velocity of light the relativistic expression for the electron's energy ($E=m_v c^2$, $m_v=m_0/[1-(v/c)^2]^{1/2}$) must be used. With $\nu'=c/\lambda'$ we have the conservation of energy,

$$h\nu + m_0c^2 = h\nu' + m_vc^2$$

conservation of momentum in the x-direction,

$$h/\lambda = (h/\lambda')\cos\phi + m_v\cos\theta$$

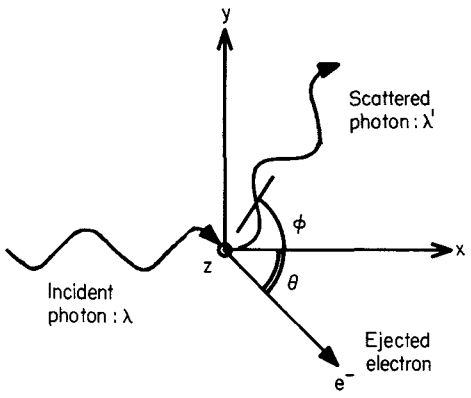

FIG. 1. Schematic diagram of the scattering of a photon by a stationary free electron.

$$\Delta\lambda = \lambda' - \lambda = (h/m_0c)(1 - \cos\phi) = (2h/m_0c)\sin^2(\phi/2) \quad (1)$$

where m_0 is the rest mass of the electron. In a grazing collision ($\phi = 0°$) there is no change in wavelength (which probably explains why Plimpton, in 1921, had concluded from his experiments on the scattering of monochromatic X-rays that there was no longer wavelength component) whereas in a head-on collision ($\phi = 180°$) $\Delta\lambda$ reaches its maximum, $2h/m_0c$. The factor h/m_0c corresponds to 0.0243 Å and is termed the Compton wavelength of the electron. Note that the inelastic Compton scattering event occurs only when the energy transferred to the electron is greater than its binding energy. When this condition is not met the X-ray photon is scattered by the entire atom (of mass M, say) and the Compton shift, $\Delta\lambda$, is diminished by a factor of m_0/M, which is c. 10^{-3}. In other words, the scattering event is then essentially elastic ($\Delta\lambda/\lambda \approx 10^{-4}$) and this accounts for the occurrence of a second peak in *Figure 2*. This interpretation was first fully articulated by Jauncey in 1924. To Jauncey also may be attributed the first clear appreciation of what has since been termed the impulse approximation, a notion that still plays an important role in the interpretation of Compton scattering data. Jauncey pictured the interaction between the photon and the scattering electron as taking place on a time scale so short that it is complete before the electron has had a chance to move in the potential well and hence to change its potential energy. The implication of this is that the bound electron may be regarded as free but with the same momentum distribution as the electron in the sample. In Section 2 we show that the impulse approximation is valid provided the energy transfer is greater than about four times the binding energy (Williams and Egerton, 1982).

In *Figure 2* it is clear that the width of the Compton scattered line is broader than could be explained by the inhomogeneity in the scattering angle or any imperfections in the X-ray spectrometer. Compton himself seemed not to have reached any firm conclusion as to the source of this broadening. The correct interpretation came, in due course, from the joint endeavours of DuMond, Kirkpatrick, Ross and Jauncey (*see*

† (*cont.* from page 40).

and conservation of momentum in the y-direction,

$$0 = (h/\lambda)\sin\phi - m_v \sin\theta$$

Eliminating v and ϕ from these equations gives

$$\Delta\lambda = \lambda' - \lambda = (h/m_0c)(1 - \cos\phi).$$

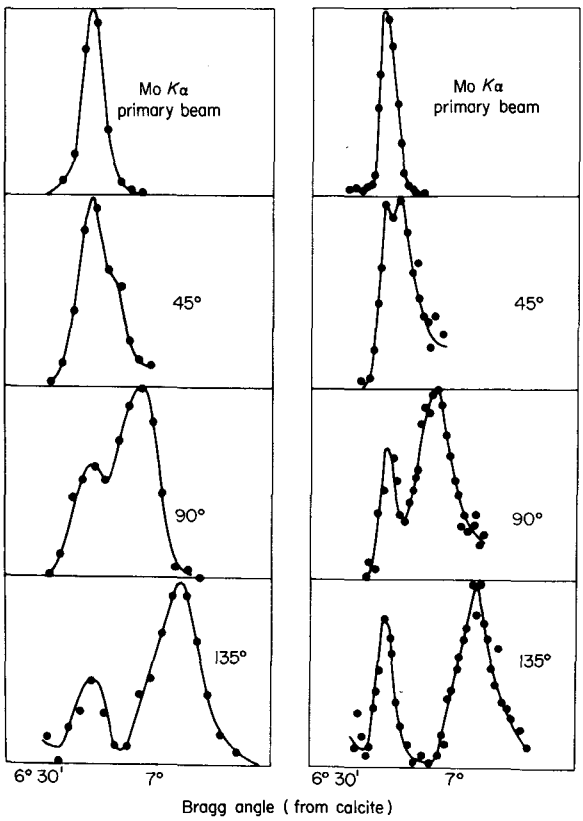

FIG. 2. Compton's data for the scattering of MoK_α X-rays from graphite (Compton, 1923). As the scattering angle increases the wavelength of the Compton line increases. In the right hand set of data Compton used narrow slits to reduce the beam divergence and deduced that the broadening of the Compton line could not be attributed solely to the spread in the scattering angle.

Steuwer, 1975; Steuwer and Cooper, 1977). Ross appears to have been the first to suggest that the momentum of the scattering electron might influence the structure of the Compton scattered line but it was DuMond (1929) who first showed that the effect of the electron's motion on the Compton scattering process could be described as a Doppler broadening mechanism rather akin to the broadening of spectral lines produced by atoms in thermal motion. As we shall discuss in Section 2 the motion of the scattering electron gives rise to a second term in Eq. (1) which becomes (Williams, 1977a)

$$\Delta\lambda = (2h/m_0c)\sin^2(\phi/2) + 2(\lambda\lambda')^{1/2}(p_z/m_0c)\sin(\phi/2) \qquad (2)$$

where p_z is the component of the electron's momentum along the scattering vector. This fuller interpretation of Compton scattering now shows that the process is dependent upon the chemical nature of the target and this is the theme which we shall develop below.

Returning to Eq. (1), it is instructive to compute the order of magnitude of the energy and wavelength changes associated with Compton scattering. If X-rays of wavelength 1 Å are scattered through 90° the wavelength change is, from Eq. (1), $\Delta\lambda = 0.0243$ Å. To

compute the kinetic energy, K, imparted to the scattering electron we write:

$$K = hc/\lambda - hc/\lambda' = hc\ \Delta\lambda/[\lambda(\lambda + \Delta\lambda)]$$
$$= 4.73 \times 10^{-17}\ \text{J} = 296\ \text{eV}$$

This value of the recoiling energy is seen to be approximately 2.3% of the original X-ray energy (12 400 eV). Since $\Delta\lambda$ does not depend on the wavelength of the incident photon, note that more energetic X- or γ-rays, with smaller wavelengths, will suffer a larger percentage increase in wavelength and also a larger percentage loss in energy. These facts, and others, are important in deciding whether to perform Compton scattering measurements with X-rays or with γ-rays. The above calculations also help us to appreciate the fact that, as the energy of the incident photon increases, the Compton process gradually dwarfs the competing photoelectric process (*Fig. 3*). The lower the atomic number of the target atoms, the sooner, in incident energy, does the Compton process dominate the photo-electric process. Irrespective of composition when the incident photon energy lies between 0.5 and 5 MeV the Compton process holds sway. At still higher incident photon energies, pair production (positrons and electrons from parent photons) takes over (*Fig. 3*).

We complete this historical section by mentioning the early theoretical formulations relevant to the interpretation of Compton line profiles. To calculate the momentum density of electrons it is first necessary to know the relevant momentum wavefunctions. Chemists are much more familiar with position wavefunctions since the square of the position wavefunction has a meaning that may readily be comprehended: it is not as easy to think intuitively in momentum space. Although some important early papers in quantum mechanics dealt directly with momentum distributions (Podolsky and

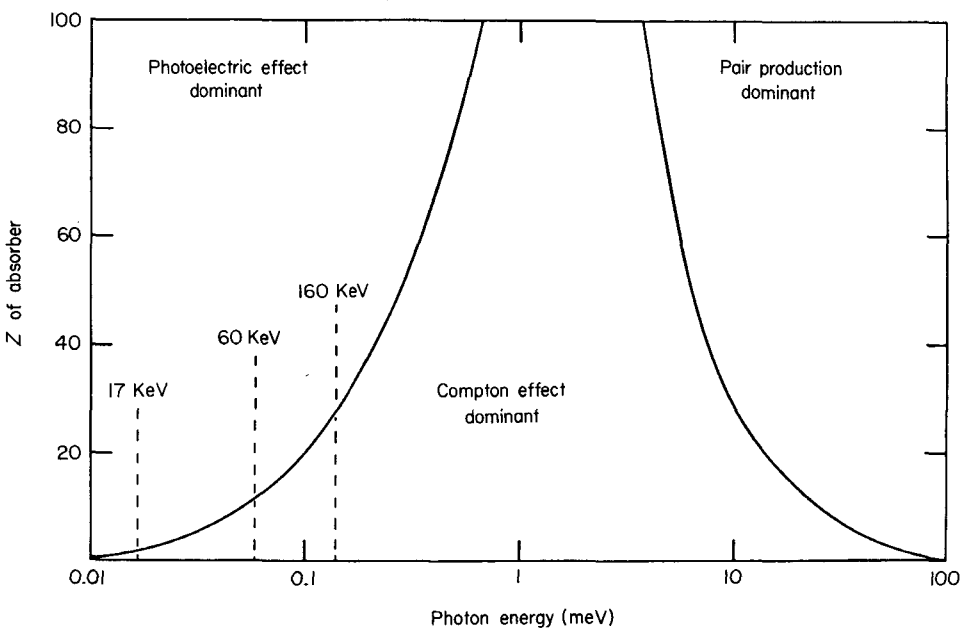

FIG. 3. The relative importance of the photo-electric effect, the Compton effect and pair production as a function of the atomic number of the sample and the energy of the incident beam. The dashed lines indicate the energies corresponding to MoK_α X-rays, Am γ-rays and Te γ-rays.

Pauling, 1929) it was not until the early 1940s that a number of seminal papers were published (Coulson, 1941; Coulson and Duncanson, 1941; Duncanson, 1941; Duncanson and Coulson, 1941, 1942) showing how to calculate the electron momentum distribution for molecules by Fourier transforming the real space (position) wavefunctions. These authors dealt with H_2, H_2^+ and some simple hydrocarbons: recently, rather more complicated molecular entities concerning a wider range of compounds have been tackled (for reviews *see* Epstein, 1973, 1975; Williams, 1977a). For solids, the computations are more demanding and this was apparent in the early work of Coulson and March (Coulson and March, 1950; March, 1954; Donovan and March, 1956). An important conclusion, which emerged clearly from March's work in this period, was the realization that Compton profiles for solids are roughly twice as wide as those of the constituent free atoms, in line with the published experimental results of DuMond (1929) and others of an even earlier era. DuMond's paper on beryllium, was extremely important since it constituted the first direct evidence in support of the free electron Fermi gas theory of metals. We shall comment further on the salient features of that work in Section 3.

Topics selected for this review

Even though we shall concentrate predominantly upon Compton scattering studies of solids reference will be made, for illustrative purposes, to scattering by atoms and by molecules. In Section 2 we outline the essentials of scattering theory for the Compton process and in Section 3, which is devoted to broad experimental features, we discuss the relative merits of X-ray, γ-ray and synchrotron sources as well as electron sources. In particular, we discuss the feasibility and merits of conducting Compton scattering experiments using appropriately adapted electron microscopes. Reference is also made to so-called (e, 2e) spectroscopy, a technique which has aroused considerable interest for the study of atoms and molecules (Moore *et al.*, 1982) and to positron annihilation techniques.

So far as the analysis and interpretation of Compton profile measurements are concerned (Section 4) we show the advantages of using the notion of the so-called reciprocal form factor, the three-dimensional Fourier transform of the momentum density. In a given direction this is synonymous with the one-dimensional Fourier transform of the Compton profile in the same direction (Weyrich *et al.*, 1979), a fact of considerable value for interpretative purposes.

So far as chemical applications are concerned (Section 5) some of the topics, concepts and properties we touch upon deal with Fermi surfaces; the spatial distribution of bonding electrons; promotion and excitation of electrons during structural phase changes; degree of charge transfer in intermetallic alloys, or between guest and a layered host, as in graphite intercalates and testing the reliability of computed wavefunctions. In this review we have chosen examples which illustrate the range of systems for which Compton scattering provides useful information and have not tried to provide an exhaustive survey of the many papers which have been published on Compton scattering. Our final section (6) dwells on the future physicochemical prospects of Compton profile studies.

2. SCATTERING THEORY

In these experiments a beam of particles is scattered from the electrons in the sample. By measuring the energy and momentum of the incident particles and of the scattered,

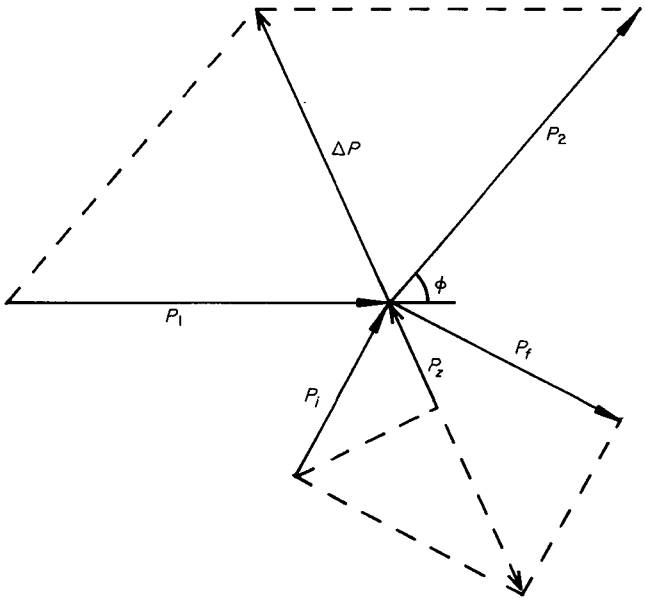

FIG. 4. Momentum conservation diagram for Compton scattering. 1 and 2 refer to the incident and scattered photons or electrons respectively, i and f to the initial and final states of the sample electron, ϕ is the scattering angle and p_z the component of $\boldsymbol{p}_i$ in the direction of $\Delta\boldsymbol{p}$.

ejected or emitted particles, and using the conservation of momentum and energy it is possible to obtain information about the ground-state momentum of the sample electrons (Williams, 1977a).

Consider an experiment in which a photon or an electron is scattered from an electron in the sample as represented schematically in *Figure 4*. The equations for the conservation of energy and momentum are

$$\boldsymbol{p}_i + \boldsymbol{p}_i = \boldsymbol{p}_2 + \boldsymbol{p}_f \tag{3}$$

$$E_1 + E_i = E_2 + E_f \tag{4}$$

where 1 and 2 denote the incident and scattered electrons or photons and i and f the initial and final states of the sample electron, each having momentum $\boldsymbol{p}$ and energy E. In (e, 2e) experiments it is possible to determine the momentum and the energy of the incident and scattered particles as well as of the ejected electron so that Eqs (3) and (4) immediately give all three components of the momentum as well as the energy of the electron that did the scattering. However, in Compton experiments only the scattered particle and not the ejected electron is detected and one must then use Eqs (3) and (4) to eliminate $\boldsymbol{p}_f$ and E_f. Assuming that E_i is the kinetic energy of the sample electron these equations lead directly to an expression for $-\Delta E$, the energy transferred from the incident particle to the electron in the sample

$$\begin{aligned} -\Delta E = E_f - E_i &= p_f^2/2m - p_i^2/2m \\ &= (\boldsymbol{p}_i - \Delta\boldsymbol{p})^2/2m - p_i^2/2m \end{aligned}$$

so that

$$-\Delta E = (\Delta p)^2/2m - \boldsymbol{p}_i \cdot \Delta \boldsymbol{p}/m \tag{5}$$

where $\Delta \boldsymbol{p}$ is the momentum transferred in the scattering process. This equation is the non-relativistic equivalent of Eq. (2) written in terms of energies so that it applies to electron scattering as well as to photon scattering. The first term on the right hand side of Eq. (5) gives the energy loss for scattering from stationary free electrons and depends only on the incident energy and the scattering angle (cf. Eq. (2)). The second term on the right hand side of Eq. (5) is proportional to the projection of the ground state momentum of the sample electron onto the scattering vector and therefore broadens the energy distribution of the scattered particles. The important point is that in any scattering process it is only the motion of the target electrons in the direction of the scattering vector that affects the energy transfer. Schematically, the measured Compton profile has the form shown in *Figure 5*. Since, to observe the Compton effect at all, the energy and momentum must be transferred to individual electrons, the energy transfer must be greater than the binding energy of the electrons in the sample. A cutoff is therefore included in *Figure 5* at an energy transfer corresponding to the binding energy.

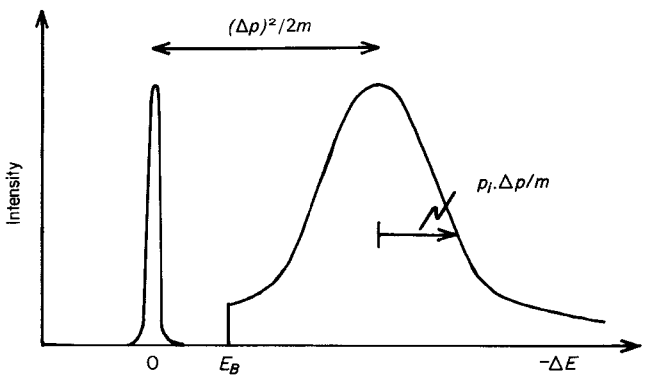

FIG. 5. Schematic representation of an experimental Compton profile. The elastic line occurs at the same energy as that of the incident beam. The Compton peak shift and broadening are given by Eq. (5). The cutoff in the profile occurs when the energy transfer is equal to the binding energy, E_B.

Having measured a Compton profile Eq. (5) may be used to convert the energy scale to a momentum scale in order to obtain the probability distribution of one component of the momentum of the electrons in the sample. To calculate the Compton profile, the theoretical momentum density must be averaged over planes in momentum space. Letting the scattering vector define the p_z direction of the coordinate system the Compton profile, $J(p_z)$, is

$$J(p_z) = \int_{-\infty}^{+\infty}\!\!\int \rho(\boldsymbol{p})\, \mathrm{d}p_x\, \mathrm{d}p_y \tag{6}$$

where the momentum density $\rho(\boldsymbol{p})$ is the square of the momentum wavefunction, $\chi(\boldsymbol{p})$

$$\rho(\boldsymbol{p}) = \chi^*(\boldsymbol{p})\chi(\boldsymbol{p}) \tag{7}$$

The momentum wavefunction is in turn the Fourier transform of the position wavefunction, $\psi(\boldsymbol{r})$

$$\chi(\boldsymbol{p}) = \iiint_{-\infty}^{+\infty} e^{-i\boldsymbol{p}\cdot\boldsymbol{r}/\hbar}\psi(\boldsymbol{r})\,\mathrm{d}\boldsymbol{r} \tag{8}$$

Experimental Compton profiles therefore provide a direct measure of the ground state wavefunction of the electrons. However, these results depend on the validity of the binary encounter impulse approximation. Using a semiclassical description this assumes that the scattering takes place so quickly that the sample electron does not move during the time of the interaction. The time during which the interaction takes place can be estimated as follows. It is impossible to conserve both energy and momentum for a process in which a free electron simply absorbs a photon. In Compton scattering, therefore, an electron absorbs a photon to create a virtual state which emits the scattered photon. Violation of the conservation of energy is then permitted provided the lifetime of the virtual state is of the order of $\hbar/\Delta E$. ΔE, the uncertainty in the energy of the virtual state is of the order of the energy of the incident photon which for 10 keV photons gives a lifetime of about 10^{-20} second. If the virtual electron travelled at the speed of light it would only move 0.01 Å before emitting the scattered photon and as the incident energy increases the lifetime decreases still further. The potential energy is then the same immediately after the collision as it was immediately before the collision, the potential energy terms in Eq. (4) cancel and the use of the kinetic energy to derive Eq. (5) is justified. In the same spirit interactions with other electrons and therefore, by definition, many-body effects are ignored in the scattering cross-section. In order to investigate further the limits of validity of this approximation a more rigorous quantum mechanical analysis is needed. Without going into the details it is instructive to consider briefly how such a calculation proceeds. Using perturbation theory for the scattering of a photon by a free electron or the Born approximation for electron–electron scattering, the scattering cross-section takes the form (Bonham and Wellenstein, 1977; Platzman and Tzoar, 1977).

$$d^2\sigma/d\Omega\,\mathrm{d}E \propto \sum_f |\langle f|e^{i\Delta\boldsymbol{p}\cdot\boldsymbol{r}}|i\rangle|^2\,\delta(E) \tag{9}$$

where $|i\rangle$ is the ground state of the sample electron and the sum is over all final states $|f\rangle$ of the ejected electron which satisfy the energy conservation delta-function. The exponential factor follows on the assumption that both the incident and the scattered photons or electrons can be represented by plane waves so that $\Delta\boldsymbol{p}$ is the momentum transferred in the scattering process. The earlier results, Eqs. (6) and (7), now follow if a plane wave final state is used for the ejected electron. Using Eq. (3) the matrix element in Eq. (9) becomes

$$\langle e^{-i\boldsymbol{p}f\cdot\boldsymbol{r}}|e^{-i\Delta\boldsymbol{p}\cdot\boldsymbol{r}}|i\rangle = \langle e^{-i\boldsymbol{p}i\cdot\boldsymbol{r}}|i\rangle = \chi_i(\boldsymbol{p}) \tag{10}$$

and the scattering cross-section is proportional to the square of the momentum wavefunction integrated over all values of the initial momentum consistent with the conservation laws. To go beyond the impulse approximation a more accurate wavefunction must be used for the ejected electron and the binding energy must be used in the energy conservation equation. Such calculations have been carried out for both X-ray Compton scattering (Mendelsohn and Smith, 1977) and more recently for electron Compton scattering (Wong *et al.*, 1982 and references therein). The very extensive electron scattering studies, both experimental and theoretical, indicate that the *impulse approximation is generally valid provided the energy transfer in the*

experiment is more than about four times the binding energy. Equations (6) to (8) can then be used to interpret Compton profile data.

3. EXPERIMENTAL METHODS

A number of different techniques involving the use of X-rays, γ-rays, electrons and positrons are commonly used to obtain information about electron momentum densities. In these experiments the intensity produced by the source varies from 10^{10} to 10^{15} particles per second. However, the recorded count rates are usually between 1 and 1000 counts per second. This enormous 'loss' of intensity follows from the need to collimate the incident and scattered beams in order to determine the various momenta with sufficient precision. It is therefore imperative to design experiments in such a way as to maximize the intensity without sacrificing resolution.

γ-ray scattering

In γ-ray experiments a radioactive source provides the incident beam and a germanium crystal, solid state detector is used to determine the energy distribution of the photons scattered through a well defined angle close to 180°, as illustrated schematically in *Figure 6.*

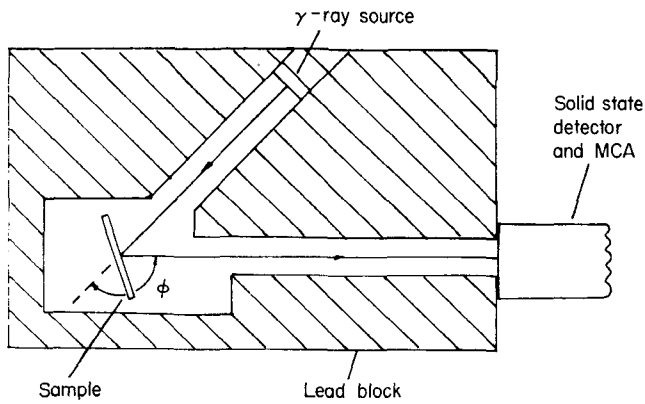

FIG. 6. Schematic diagram of a γ-ray Compton scattering spectrometer.

Since both the incident energy and the energy transfer may be of the order of 100 to 400 keV it is necessary to use the relativistic version of Eq. (5). The most convenient form of this equation for photon scattering is (Weiss *et al.*, 1977)*

$$p_z=[\Delta E-E_iE_f(1-\cos\phi)]/[E_i^2+E_f^2-2E_iE_f\cos\phi]^{1/2} \qquad (11)$$

where ϕ is the scattering angle.†

* Note that this and some subsequent equations will be written in Compton atomic units for which $m=1$, $c=1$, $\hbar=1$ and $e=1/\sqrt{137}$. In conventional atomic units, referred to simply as atomic units, $m=1$, $\hbar=1$, $c=137$ and $e=1$.

† Equation (11) reduces to Eq. (5) if the square root is expanded and terms of order $(\Delta E/E)^2$ and higher are neglected.

The cross-section for the scattering of photons by electrons is given approximately by the Thompson cross-section

$$\sigma = r_0^2 \boldsymbol{e}_1 \cdot \boldsymbol{e}_2 \tag{12}$$

where $r_0 = e^2/mc^2$ is the classical electron radius and $\boldsymbol{e}_1$ and $\boldsymbol{e}_2$ are the polarization vectors of the incident and scattered photons. In order to ensure that most of the electrons are scattered at least once, the sample must be of the order of 1 mm to 1 cm thick. Furthermore, at low photon energies photoelectric absorption attenuates the beam significantly so that the incident energy should be of the order of 50 to 500 keV, depending on the atomic number of the sample. The use of high energies and angles ensures that the energy transferred in the scattering process is of the order of 10 to 100 keV so that the binary encounter, impulse approximation, which is used to relate experimental profiles directly to the ground state wavefunction, is valid.

A number of sources having an isolated line of suitable energy are available (DuBard, 1979). Those most commonly used are ^{241}Am with a line at 60 keV (Manninen and Paakkari, 1978; Bonse *et al.*, 1979), ^{51}Cr with a line at 320 keV (Lässer *et al.*, 1979), and ^{198}Au with a line at 412 keV (Pattison and Schneider, 1979). ^{241}Am has a half-life of 458 years but self-absorption in the source material is high and the activity is limited to about 1 Ci/Cm^2 (10^{10} γ/second). ^{51}Cr has a half-life of 27 days and source strengths of about 50 Ci can be obtained while ^{198}Au has a half-life of only 2.7 days but activities of 200 Ci (10^{12} γ/second) are regularly obtained. *Figure* 7 shows a Compton profile of graphite measured by us using a ^{51}Cr source of about 50 Ci over a period of 24 hours.

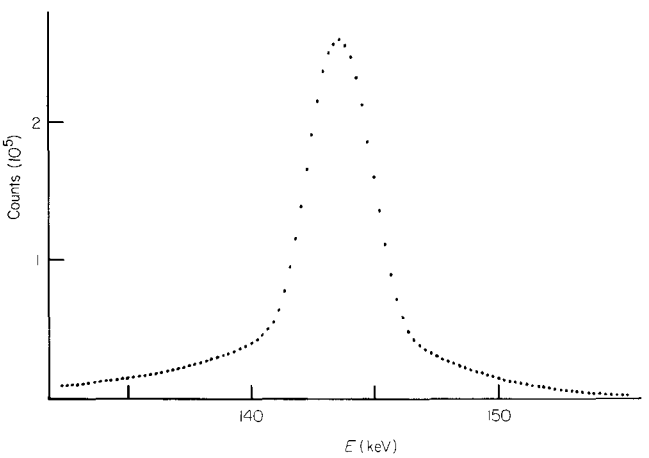

FIG. 7. γ-ray Compton profile data for ^{51}Cr (320 keV) radiation scattered through 165° from graphite. The experimental data have been summed in groups of four channels.

The energy resolution in these experiments depends on the band gap of the solid state detector which determines the number of electron–hole pairs created each time a photon is detected. The energy resolution varies as the square root of this number and is therefore proportional to $E^{1/2}$ while, for low energies, the width of the Compton profile increases linearly with the photon energy (Eq. (11) with $E_f \approx E_i$, $\phi = 180°$) so that the Compton resolution improves as the energy is increased (Williams, 1977b). However as one approaches higher energies (c. 511 keV $= mc^2$) relativistic terms in Eq. (11) become

more important and for 180° scattering beyond 511 keV the momentum resolution becomes worse with increasing incident energy. Even at high energies and for scattering angles close to 180° the resolution is far from ideal and is about 0.35 a.u. for Au sources (412 keV) while valence electron Compton profiles are typically about 2 a.u. wide (Williams, 1976, 1977b).

The divergence of the incident and scattered beams introduces a further contribution to the resolution (Williams, 1977b). In order to maximize the scattered intensity without degrading the resolution more than is necessary, the spread in scattering angles must be chosen so that the additional broadening is not more than about 20% of the resolution provided by the detector. Again it is advantageous to use a high incident energy and a scattering angle as close to 180° as possible but of course it is also necessary to shield the detector from the source and a compromise of about 165° with a divergence angle of about 2° is usually chosen.

A number of γ-ray spectrometers have been designed using these criteria and further details are available in the literature (Manninen and Paakkari, 1978; Pattison and Schneider, 1979).

X-ray scattering

In order to overcome the rather severe limitations imposed by the resolution of γ-ray detectors there is considerable interest at present in the use of X-ray sources and crystal spectrometers. Indeed, between 1960 and 1970 almost all photon Compton scattering experiments were carried out using X-rays. In these experiments a fluorescence X-ray tube provided the incident beam and a Bragg spectrometer was used to carry out a wavelength analysis of the scattered radiation (Weiss *et al.*, 1977). Unfortunately, these experiments suffered from two crucial limitations. The use of X-ray tubes meant that a large Bremstrahlung background was present and because the spectrum had to be scanned point by point the observed count rates were often as low as 1 count/second. The development of synchrotron radiation as a source of X-rays and developments in the use of electronic position sensitive detectors in conjunction with curved crystal spectrometers now makes this technique much more attractive. *Figure 8* is a schematic

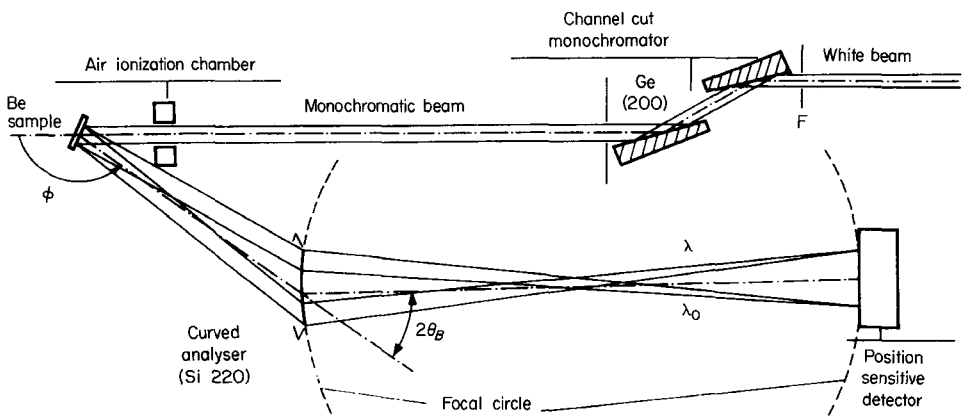

FIG. 8. Schematic diagram of a Compton spectrometer for use with a synchrotron source. A germanium channel-cut crystal monochromates the incident beam. The scattered beam is analysed using a curved crystal and a position sensitive detector (Loupias *et al.*, 1980).

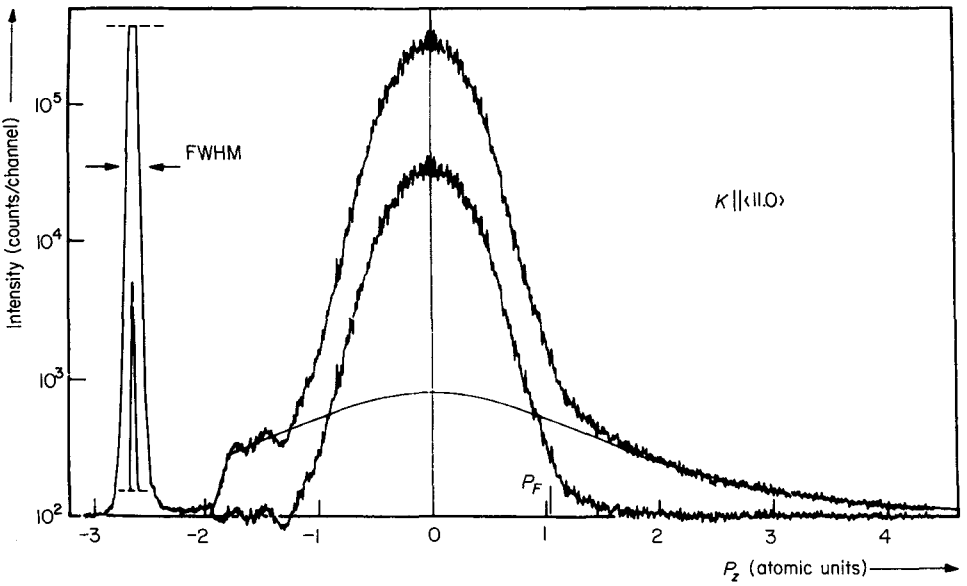

FIG. 9. X-ray (synchrotron) Compton profile of beryllium. The wavelength resolution corresponds to 0.15 a.u. of momentum. In the lower curve a free atom Compton profile for the core electrons in the impulse approximation (smooth line) has been subtracted from the data (Loupias *et al.*, 1980).

diagram illustrating the geometry of the experiment and *Figure 9* shows the results of one of the first experiments using this technique to measure the Compton profile of beryllium (Loupias *et al.*, 1980; Loupias and Petiau, 1980). The data in *Figure 9* were measured with a resolution of 0.15 a.u. Using synchrotron radiation the flux decreases very rapidly with increasing energy and in this experiment an energy of 10 keV was used. For heavy elements and low incident energies photoelectric absorption reduces the scattered intensity quite considerably (*see Fig. 3*) so that this technique will be most suitable for the study of samples consisting of light elements.

When an X-ray or γ-ray Compton profile has been measured, the data are converted to a momentum scale using Eq. (11). A number of corrections must then be applied to the data to allow for the energy dependence of absorption in the sample, energy dependent terms in the cross-section, the detector efficiency and so on (Williams, 1976; Weiss *et al.*, 1977). The most problematical correction arises from the presence of multiple scattering. In order to maximize the observed count rates the sample should be large enough to ensure that most of the photons are scattered at least once but a significant fraction of photons will then be scattered two or more times. It is rather difficult to calculate the intensity and spectral distribution of multiple scattering events from first principles although computer programs based on Monte Carlo techniques are available (Halonen *et al.*, 1977). However, one can make a number of general observations which provide some insight into the nature of the problem. The dominant contribution to multiple scattering arises from double scattering events in which each is a Compton collision. Since double Compton scattering is essentially the convolution of two single Compton scatterings, it can be shown that for a Gaussian Compton profile and 180° scattering, the contribution from such events is identical to the single scattering profile (Williams *et al.*, 1974). For scattering angles below 180° this double scattering contribution becomes wider and skewed towards the low energy side of the

profile (Williams *et al.*, 1974). To correct for the effects of multiple scattering one can either carry out measurements on samples of varying thickness and extrapolate to zero thickness (Paatero and Halonen, 1976), or use a Monte Carlo technique to calculate the multiple scattering from first principles or, alternatively, use some combination of the two approaches (Halonen *et al.*, 1977). It is important to note that since the multiple scattering depends on the geometry of the sample, great care must be taken when using difference measurements to study anisotropies.

Electron scattering

Electron scattering provides a very attractive alternative to photon scattering for the study of electron momentum densities (Bonham and Wellenstein, 1977). The incident beam intensity may be as high as 10^{15} electrons per second (100 μA) and the cross-section under typical experimental conditions is several orders of magnitude greater than the photon scattering cross-section. The high count rates together with the fact that electrons are being detected makes it possible to observe the ejected electron in coincidence with the scattered electron (Furness and McCarthy, 1973; Moore *et al.*, 1982). It is then possible to determine the momentum density directly without integrating over planes and also to use energy conservation to separate out the contributions from electrons in different energy levels. Alternatively, experiments can be carried out in an electron microscope making it possible to combine the momentum density with images, diffraction patterns and other electron energy-loss experiments (Williams *et al.*, 1981). However, electron scattering experiments are not without their limitations which arise principally from multiple scattering and radiation damage.

In electron scattering experiments the design criteria are essentially the same as in the γ-ray case but the way in which these are met leads to different experimental geometries. Incident beam energies are between 20 and 200 keV so that it is again necessary to include relativistic terms in the expression for the energy loss and, in Compton atomic units, Eq. (5) now takes the form (Williams *et al.*, 1981)

$$-\Delta E = -\Delta E_0 + p_z(2\,\Delta E_0)^{1/2} \tag{13}$$

with

$$\Delta E_0 = E_i(1 + E_f/2)\sin^2\phi \tag{14}$$

The crucial differences between electron and photon scattering experiments arise from the strength of the interaction and the angular dependence of the cross-section. For photons the cross-section is almost isotropic whereas for electrons the scattering cross-section is given by

$$\sigma = r_0^2/\Delta E_0^2 \tag{15}$$

where r_0 is the classical electron radius and ΔE_0 is in units of mc^2. The electron scattering cross-section therefore depends only on the energy transfer to the Compton peak but for a fixed incident energy decreases as the fourth power of the scattering angle. Comparing Eqs (12) and (15) for an energy transfer to the Compton peak of 1 keV the electron scattering cross-section is about 10^5 times the photon scattering cross-section so that solid samples must be between 100 and 1000 Å thick. In order to maximize the scattered intensity it is important to keep the energy transfer as low as possible consistent with the binary encounter impulse approximation. *Figure 10* is a schematic diagram of an electron scattering (gas phase) Compton spectrometer. In order to minimize radiation damage and multiple scattering most electron scattering

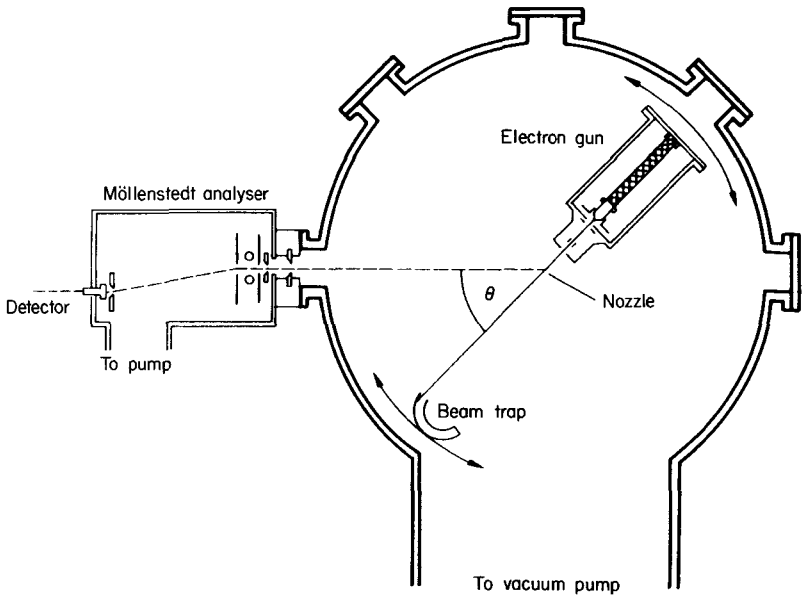

FIG. 10. Schematic diagram of a gas-phase electron Compton scattering spectrometer (Bonham and Wellenstein, 1977). The sample gas jet intersects the electron beam at right angles.

experiments have been carried out using a low pressure jet of gas for the sample. An electron gun provides a 20 kV incident beam which intersects the sample jet at right angles. The energy spectrum of the electrons scattered through an angle of about 10° is measured using a Möllenstedt analyser. The energy transfer to the Compton peak is typically 500–1000 eV. *Figure 11* shows an experimental Compton profile of helium. To obtain a momentum resolution of 0.1 a.u. an energy resolution of 20 eV is required and this is readily attainable (Williams *et al.*, 1981). The angular resolution is more problematical. For an incident energy of 100 keV and a momentum resolution of 0.1 a.u. the angular divergence must be of the order of 0.06° (1 mrad) or alternatively for an energy loss to the Compton peak of 1 kV the spread in scattering angles must be of the order of 1% of the scattering angle. The use of large scattering angles with this high degree of collimation means that the available intensity is very much less than in other electron scattering experiments.

Electron scattering Compton profile measurements have also been made on solids using an electron microscope fitted with a magnetic prism spectrometer (Williams *et al.*, 1981; Williams and Bourdillon, 1982) as illustrated in *Figure 12*. The objective lens focuses the electron beam onto the sample and the objective aperture is used to limit the divergence of the incident beam. Tilt coils are used to obtain a scattering angle of about 5°. A second aperture is used to limit the divergence of the scattered beam which is focused onto a magnetic prism spectrometer.

With solid samples the problems of multiple scattering and radiation damage can no longer be entirely avoided and these will ultimately constrain the application of this technique. However, Compton profiles of amorphous carbon, graphite and aluminium have been measured in this way as illustrated for amorphous carbon in *Figure 13*. The most serious problem associated with electron Compton scattering from solids is that of radiation damage. The critical dose for radiation damage varies enormously from

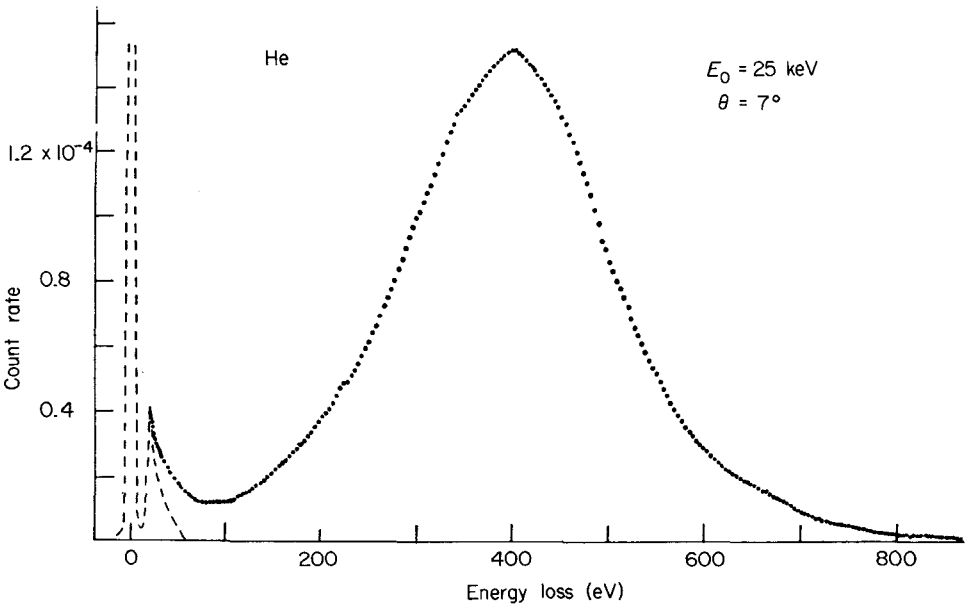

FIG. 11. Electron scattering Compton profile of helium (Bonham and Wellenstein, 1977). The small peak close to the zero loss line indicates the amount of multiple scattering.

sample to sample and depends on the criterion used to measure it. Values reported in the literature range from 0.005 C m^{-2} for polyethylene (Jones and Thomas, 1979) to 8000 C m^{-2} for copper phthalocyanine (Egerton, 1980). Using the Rutherford cross-section, Eq. (15), for a peak shift of 1000 eV and a fractional spread in the scattering angle of 1% the cross-section is $10^{-8}\ a_0^2$. With a film of carbon 200 Å thick the probability of obtaining a Compton event is then 10^{-6}. In an accurate experiment it is necessary to collect 10^6 electrons over the whole Compton profile so that 10^{12} electrons must strike the sample. For an area of 10 μm on a side this gives a dose of about 1000 C m^{-2} which for beam sensitive materials is too great by a factor of about 10^3 to 10^4. This already assumes that the entire spectrum is being observed simultaneously using a parallel detection system, but it might be possible to gain a factor of about 100 by using an annular aperture and in principle one could scan the sample so that new areas are exposed to the beam.

In electron scattering experiments the main contribution to multiple scattering is maximal near the elastic line and decreases fairly rapidly with increasing energy loss (Wellenstein *et al.*, 1973; Barlas *et al.*, 1978) so that the amount and importance of multiple scattering may be easily assessed from the raw data as can be seen in *Figure 13*. For solid samples and especially those containing heavy atoms, multiple scattering events may easily swamp the single scattering events even with samples less than 100 Å thick. It is almost certainly prohibitively difficult to calculate the multiple scattering contribution directly but it should be possible to parameterize the multiple scattering on the basis of measurements carried out on a range of samples of varying thickness and with several different incident energies and scattering angles.

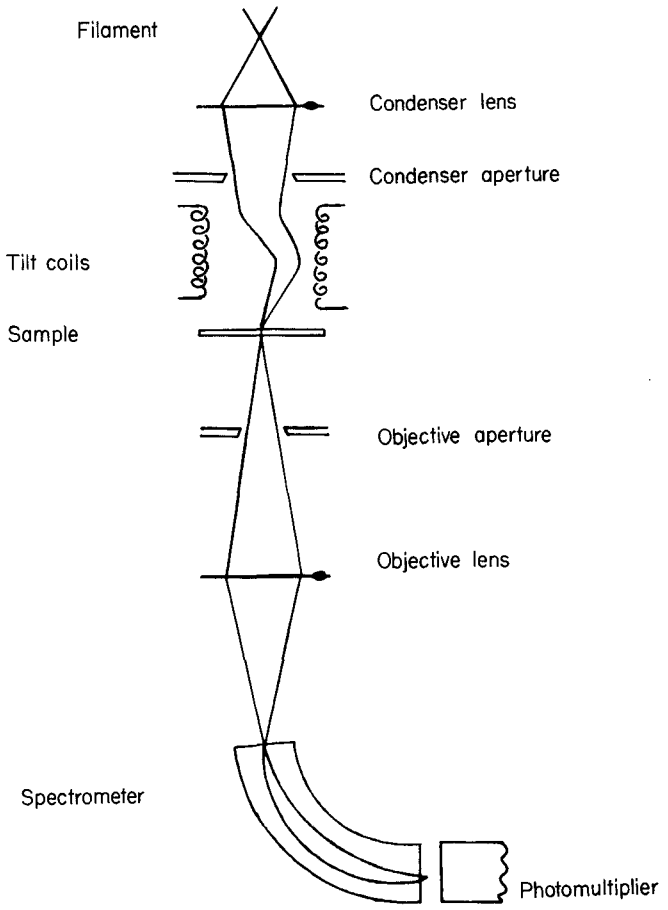

FIG. 12. Schematic diagram of an electron microscope used for Compton scattering experiments. The tilt coils are used to obtain a scattering angle of about 5° and the apertures limit the beam divergence. A magnetic prism spectrometer is used to measure the energy of the scattered electrons.

(e,2e) Scattering

In (e,2e) scattering, which we will mention only briefly, the ejected electron is detected in coincidence with the scattered electron (Furness and McCarthy, 1973; Moore *et al.*, 1982). The apparatus consists of a pair of electron energy analysers together with the appropriate coincidence circuits and hardware to collect the data. In these experiments very low incident energies are used, typically 400–1000 eV. The binary encounter impulse approximation is then no longer strictly valid and the analysis of the data in terms of $\rho(\boldsymbol{p})$ becomes rather involved. However, the analysis is facilitated if a symmetrical geometry is used in which the ejected electron and the scattered electron both emerge at 45° to the incident beam direction with about the same energy (Bonham and Wellenstein, 1977). Since this is a coincidence experiment the statistical accuracy is considerably reduced but, as noted above, there are two crucial advantages. The momentum distribution is obtained without integrating over planes and the energies of the observed particles can be used to determine the energy of the electron that did the

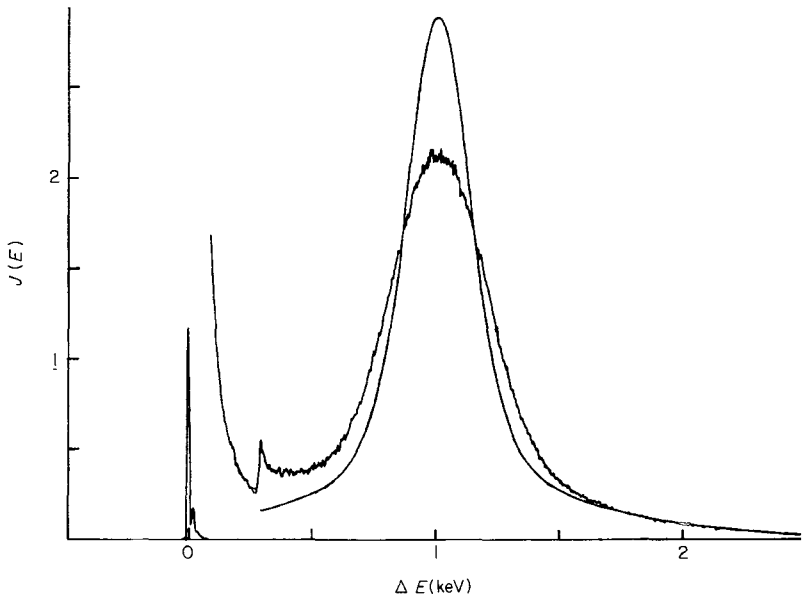

FIG. 13. Electron scattering Compton profile of amorphous carbon measured using an electron microscope. The plasmon line can be seen close to the zero-loss line and the K-edge occurs at 284 eV. The smooth line gives the Compton profile for a free atom of carbon and the difference between this and the experimental data illustrates the change in the Compton profile when the solid is formed.

scattering. *Figure 14* shows the results of an experiment on argon in which the momentum density of the 3s and the 3p orbitals have been measured separately (Weigold *et al.*, 1973).

Positron annihilation

The last of the techniques discussed here involves the measurement of the angular correlation of two photon positron annihilation (Berko, 1977; Mijnarends, 1979; West, 1980). Incident beam intensities are about 10^{10} positrons/second. The positrons thermalize before they annihilate and then annihilate preferentially with the emission of two photons. The most important competing effect is positronium formation which depends on the physical state of the sample. The scattering geometry is based on the observation that if a stationary electron–positron pair annihilates, the two photons must be emitted in opposite directions each with energy mc^2 and momentum mc in order to conserve energy and momentum. Now if the electron–positron pair has non-zero momentum immediately before the annihilation takes place the two photons will be given off at an angle which deviates from 180° in such a way as to conserve momentum as illustrated in *Figure 15*. The angle between the two γ-rays differs from 180° by 7 milli-radians per atomic unit of momentum so that for a resolution of 0.1 a.u. the spread in the angle must be about 0.7 mrad. Two components of momentum may be determined by measuring the angle between the annihilation photons in the plane of the paper and at right angles to the plane of the paper. The third component of momentum gives rise to a Doppler shift in the direction of emission of the photons and this can be measured using a solid state detector of the kind used in γ-ray scattering

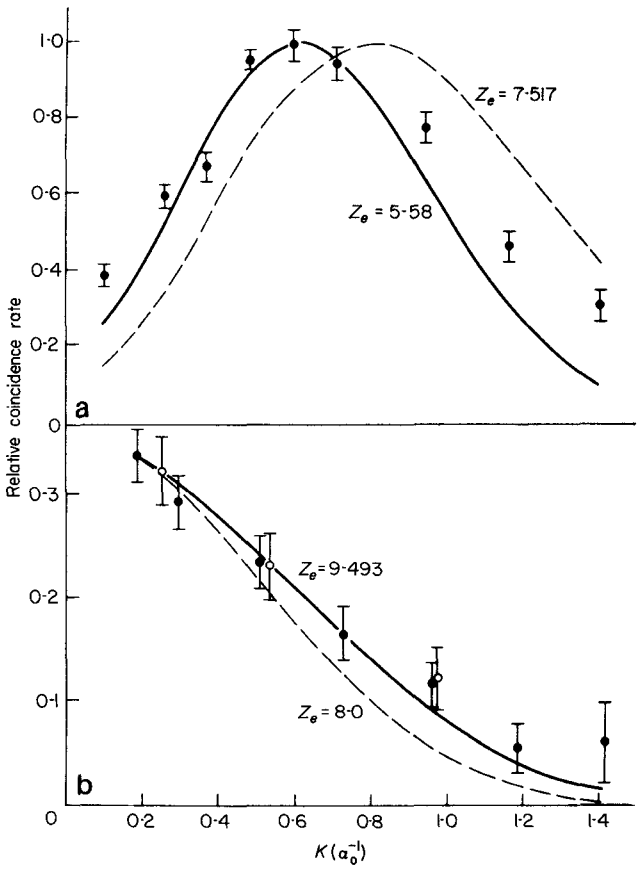

FIG. 14. Electron momentum densities for (a) the 3p and (b) the 3s states of argon measured using (e,2e) scattering of 400 eV electrons (Weigold *et al.*, 1973). The lines give theoretical densities calculated using hydrogenic wavefunctions with the effective charges shown in the figure.

experiments. However the resolution attainable in this way is only about 0.6 a.u. (Shizuma *et al.*, 1980).

The apparatus used to measure the angular correlation profiles is shown schematically in *Figure 16* and consists of a positron source, usually ^{22}Na or ^{64}Cu, sample, collimators, either point apertures or slits and NaI detectors. Using long slits only one component of the momentum is measured. Using point apertures two components of the momentum may be measured simultaneously making it possible to extract considerably more information. Systems based on the use of arrays of detectors (Berko and Mader, 1975) as well as positron sensitive Anger camera detectors (West *et al.*, 1981) are now being used and provide much faster rates of data collection.

The principal drawback of positron annihilation for the determination of electron momentum densities lies in the fact that the experiment yields the momentum density of the combined electron–positron system. To make accurate quantitative comparisons between theory and experiment a positron wavefunction must be included. Since the positron carries a positive charge it is repelled from the atomic nuclei and the annihilation is consequently biased in favour of the valence electrons and against the

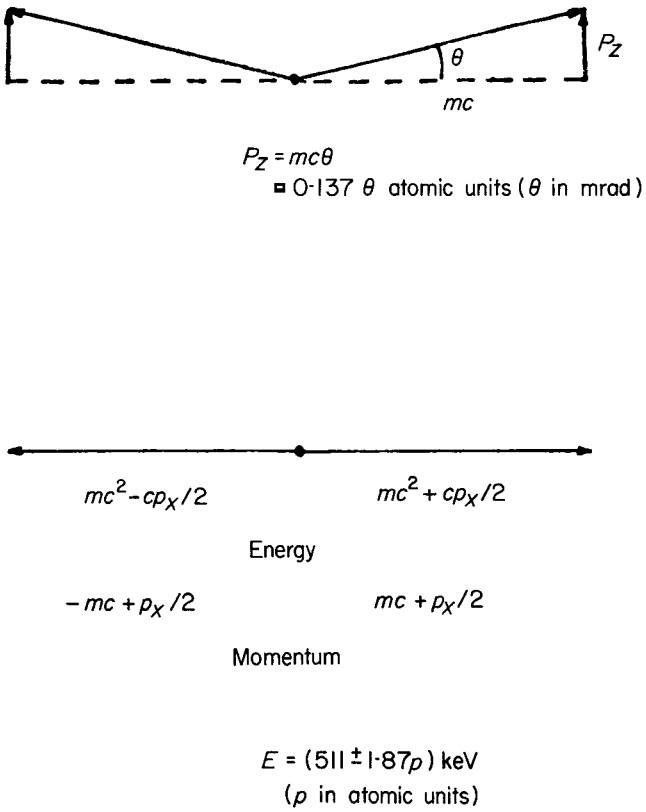

FIG. 15. Energy and momentum conservation in 2-photon positron annihilation. The electron–positron pair has energy $2mc^2$. Conservation of energy and momentum determines the angle between the two photons and the Doppler shifts of the photons.

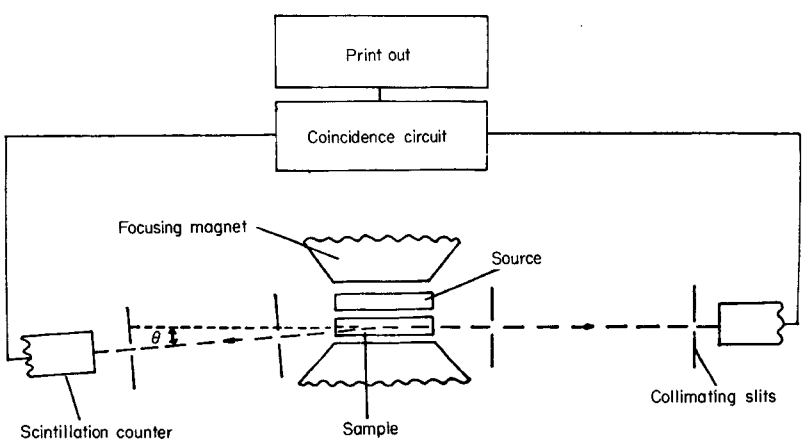

FIG. 16. Schematic diagram of the apparatus used in angular correlation measurements of 2-photon positron annihilation. One of the detectors is translated sideways and the coincidence count rate is measured as a function of the angle θ.

core electrons. Furthermore, if there is a transfer of charge the annihilation takes place preferentially with the negatively charged species. Consequently, the annihilation profiles of LiH and NaH, for example, are almost indistinguishable (Shizuma *et al.*, 1980). This then is the most important difference between positron annihilation and Compton scattering experiments. However, the effects of the positron can sometimes be turned to advantage as will be shown below in the discussion of graphite intercalates. To illustrate the quality of the data one can obtain in positron annihilation experiments, a pair of profiles for two directions of copper are shown in *Figure 17* (Fujiwara and Sueoka, 1966). The details of the Fermi surface are clearly evident and the small contribution from annihilation with core electrons as compared to the conduction electrons illustrates the effect of the positron wavefunction.

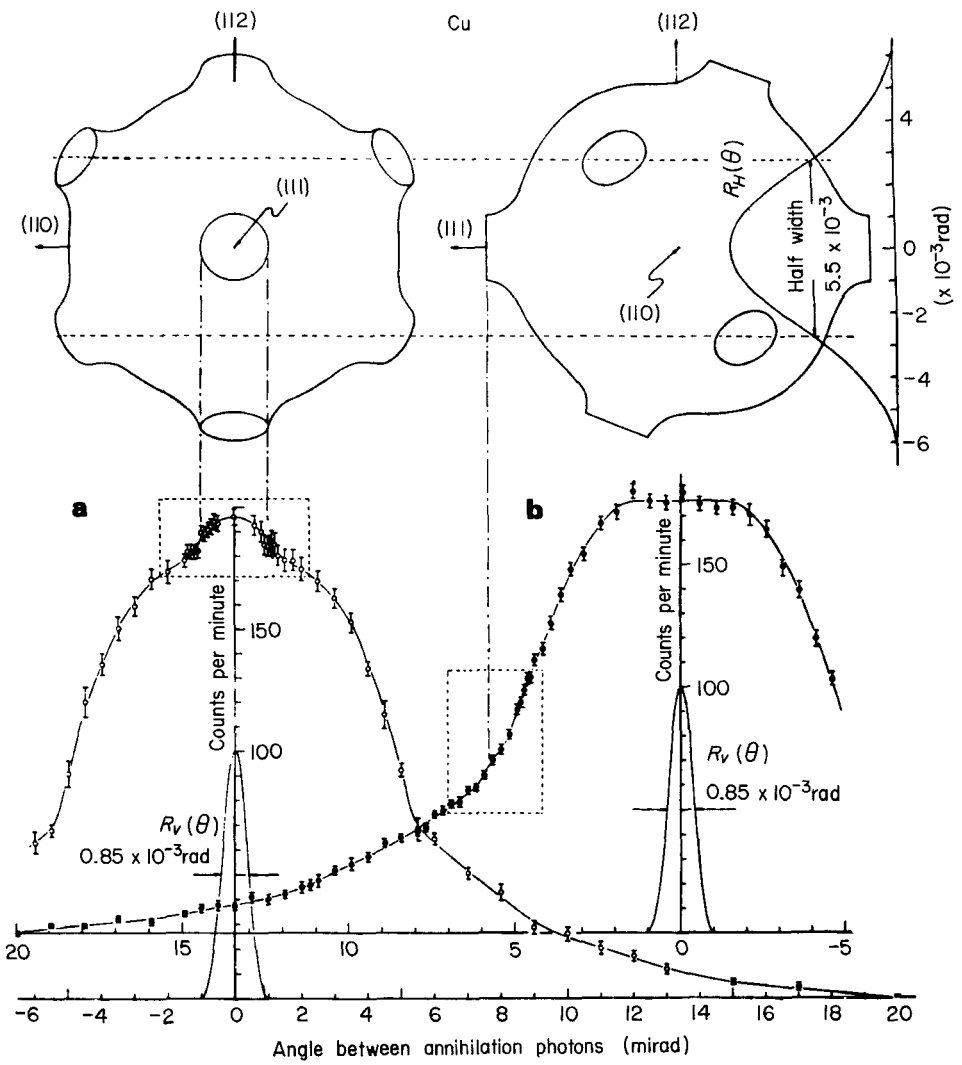

FIG. 17. Angular correlation profiles for copper. The angular resolution and the Fermi surface are also shown (Fujiwara and Sueoka, 1966).

4. ANALYSIS AND INTERPRETATION OF COMPTON PROFILES

Most quantum mechanical calculations are carried out in position space so that the simplest way to approach momentum space is to apply the theorems of Fourier transforms to the position space wavefunction. Although this provides insight into the behaviour and properties of electron momentum densities and Compton profiles (Tanner and Epstein, 1977) it is still difficult to think intuitively in momentum space. For this reason, the analysis of both experimental and theoretical data is often facilitated by Fourier transforming the Compton profile to obtain the so-called reciprocal form factor which will be a function of position. To recapitulate briefly, the important equations relating the momentum wavefunction, $\chi(\boldsymbol{p})$, the momentum density, $\rho(\boldsymbol{p})$ and the Compton profile, $J(p_z)$, one to another, are

$$\chi(\boldsymbol{p}) = \{\psi(\boldsymbol{r})\}_3 \tag{16}$$

$$\rho(\boldsymbol{p}) = |\chi(\boldsymbol{p})|^2 \tag{17}$$

$$J(p_z) = \iint_{-\infty}^{+\infty} \rho(\boldsymbol{p})\, \mathrm{d}p_x\, \mathrm{d}p_y \tag{18}$$

where $\{\ \}_N$ indicates an N-dimensional Fourier transform. Using $B(z)$ to denote the Fourier transform of the Compton profile in the direction p_z,

$$B(z) = \{J(p_z)\}_1 \tag{19}$$

or with Eq. 18

$$B(z) = \int_{-\infty}^{+\infty} e^{ip_z z} \iint_{-\infty}^{+\infty} \rho(\boldsymbol{p})\, \mathrm{d}\boldsymbol{p} \tag{20}$$

Since $\boldsymbol{p} \cdot \boldsymbol{z} = p_z z$ and the z direction of the coordinate system can be chosen to lie in the direction r

$$B(\boldsymbol{r}) = \iint_{-\infty}^{+\infty} e^{i\boldsymbol{p}\cdot\boldsymbol{r}} \rho(\boldsymbol{p})\, \mathrm{d}\boldsymbol{p} = \{\rho(\boldsymbol{p})\}_3 \tag{21}$$

Equations (19) and (21) state an important result, namely that *the 3-dimensional Fourier transform of the momentum density in a given direction is synonymous with the 1-dimensional Fourier transform of the Compton profile in the same direction* (Williams, 1971; Meuller, 1977). This leads directly to a method for the reconstruction of the 3-dimensional density. The 1-dimensional Fourier transforms of a set of directional Compton profiles are calculated and these are used to construct the 3-dimensional function, $B(\boldsymbol{r})$. The 3-dimensional transform of $B(\boldsymbol{r})$ then gives the 3-dimensional momentum density; computer programs to perform this reconstruction are available (Mijnarends, 1977; Hansen, 1981). Since the Fourier transform of the charge density is called the form factor, Weyrich has coined the term 'reciprocal form factor' to describe $B(\boldsymbol{r})$. Now the Fourier transform of a product is the convolution of the Fourier transforms so that Eqs (16) and (21) give

$$B(\boldsymbol{r}) = \psi^*(\boldsymbol{r}) \otimes \psi(\boldsymbol{r}) \tag{22}$$

where $\otimes$ signifies convolution.

In the remainder of this section the properties of Compton profiles and reciprocal form factors of atoms, molecules and solids will be discussed as a prelude to the consideration of some recent applications and examples.

Atoms

The angular symmetry of a function is preserved under a Fourier transform so that polar diagrams of atomic orbitals in position space can be carried over directly to momentum space. For 1s orbitals the momentum density is therefore spherically symmetric and the Compton profile and the reciprocal form factor decrease monotonically as r increases from zero (*Fig. 18*). For 2p orbitals the wavefunctions and densities have lobes pointing in opposite directions. Integrating the momentum density over planes in momentum space the Compton profile is bimodal in the orbital direction but shows a single peak at right angles to the orbital direction. The reciprocal form factor decreases monotonically with increasing distance at right angles to the orbital direction but in the direction of the orbital it shows a negative dip when the positive and negative lobes overlap (*Fig. 18*).

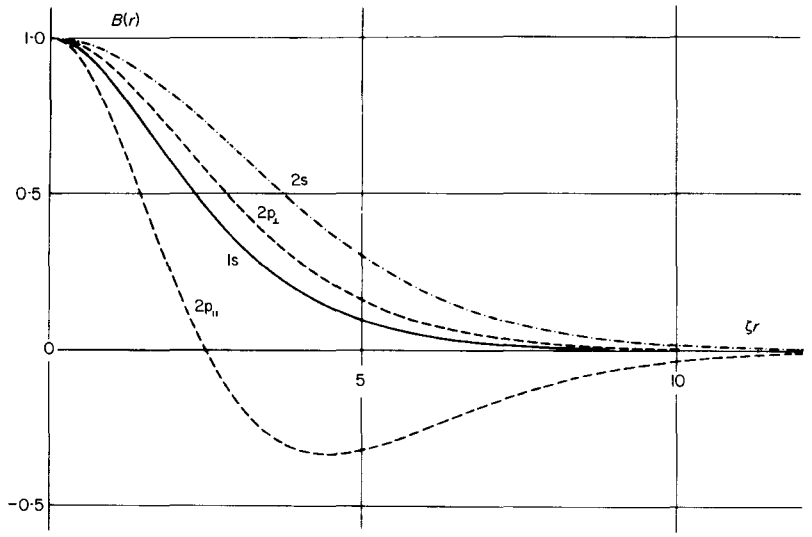

FIG. 18. Reciprocal form factors for 1s, 2s and 2p Slater orbitals. ζ is the orbital exponent. The subscripts $\parallel$ and $\perp$ refer to the direction relative to the axis of the 2p orbital (Weyrich *et al.*, 1979).

If a function is expanded its Fourier transform is contracted and vice versa. In position space the tightly bound core orbitals are highly localized while the loosely bound valence orbitals are spread out and in the reciprocal form factor the core electron contribution will be dominant at small correlation distances while the valence electrons will determine the behaviour at large correlation distances (Weyrich *et al.*, 1979). In momentum space, on the other hand, the core electrons will give a broad, flat contribution to the Compton profile while the valence electrons will contribute a relatively narrow peak.

Molecules

Perhaps the most convenient approach to molecules is by way of linear combinations of atomic orbitals. Each atomic orbital contributes to the momentum wavefunction as it does for atoms but the additional effect of multicentred functions must be included. If

a function is shifted its Fourier transform is multiplied by a phase factor. Consequently the individual momentum densities and Compton profiles will be centred at the same origin but will be modulated by phase factors which depend on the relative shifts of the atomic orbitals making up a given molecular orbital. This can be illustrated most simply by considering bonding and anti-bonding orbitals for H_2^+ (*Fig. 19*) in which the molecular position wavefunction is taken to be the sum or difference of atomic 1s orbitals centred at each atom. The momentum density $\rho(\boldsymbol{p})$ is then the atomic $\rho(\boldsymbol{p})$ multiplied by a phase factor $(1+\cos \boldsymbol{p} \cdot \boldsymbol{R})$ where R is the bold length. For the bonding orbital the momentum density is a maximum at the origin while for the anti-bonding orbital it is zero at the origin, giving rise to the position and momentum densities illustrated in *Figure 19*.

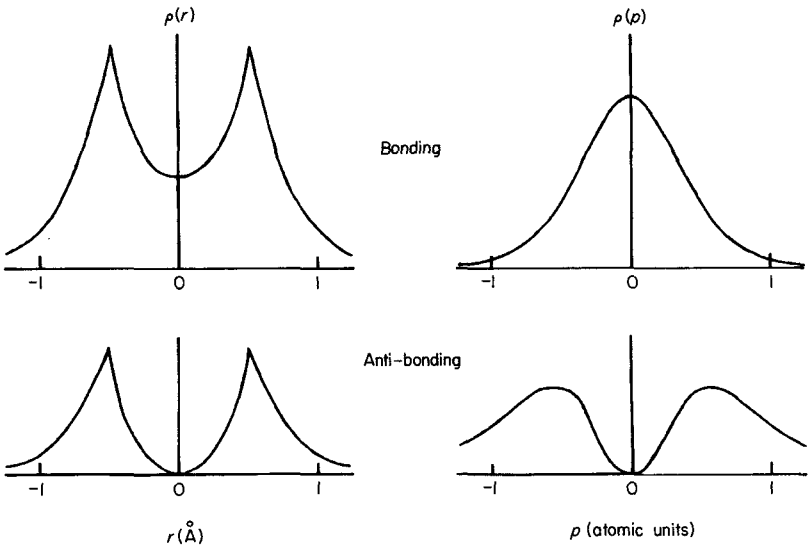

FIG. Position and momentum densities for the bonding and anti-bonding orbitals of H_2^+ in the bond direction.

The behaviour of the reciprocal form factor may be illustrated using a localized orbital, minimum basis set wavefunction for a C–C sigma bond in ethane. The sp^3 hybrids forming the bond orbital are represented schematically in the inset to *Figure 20*. The maximum negative overlap will occur when the bond orbital is displaced by the bond length and the reciprocal form factor (*Fig. 20*) shows a significant negative dip close to the bond length.

Insulating solids

LCAO wavefunctions can also be used to describe non-conducting solids. For crystalline solids the symmetry provides us with an important theorem of wide applicability. In the independent particle model the reciprocal form factor for insulators is identically zero at the lattice vectors. A proof of this theorem based on the orthogonality of Wannier functions has been provided by Schülke (1977). An alternative proof runs as follows. For a system with filled Brillouin zones the momentum density in the repeated zone scheme is constant. Now the Compton profile

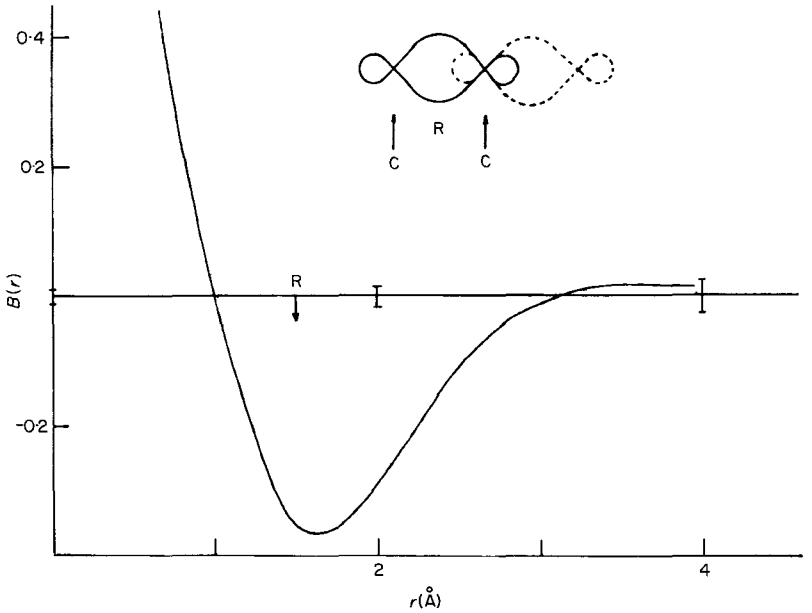

FIG. 20. Reciprocal form factor for the C–C sigma bond in ethane calculated from a localized orbital, minimum basis set wavefunction. The orbital is shown schematically in the inset (Williams *et al.*, 1983). R is the bond length.

already entails an integral over two directions in momentum space so that if it is repeatedly shifted by the lattice spacing in the direction of the measurement and all of these shifted profiles are added together, the result will be the momentum density in the repeated zone scheme which is constant, i.e.,

$$\sum_G J(p+G) = \text{constant} \tag{23}$$

Taking the Fourier transform of both sides of Eq. (23) leads immediately to the result that $B(L)=0$ for all lattice vectors, L, excluding the origin. It is the overlap between atoms in neighbouring unit cells that produces the constant density in the repeated zone scheme and hence the zeros in the reciprocal form factor at the lattice spacings. *Figure 21* shows experimental data for silicon and the reciprocal form factor does go to zero at the lattice spacings (Tejedor, 1979). This provides an excellent check on the reliability of experimental data and the validity of the orthogonalization procedures used to calculate theoretical wavefunctions.

Metals

For metals the most important feature of the momentum density is the Fermi surface. For a free electron Fermi gas this is a sphere in momentum space and the momentum density is constant inside the sphere and zero outside of it. Integrating over planes, the Compton profile for a Fermi gas is an inverted parabola cutting off at the Fermi momentum. As one would expect this provides a reasonably accurate model for the Compton profile of sodium illustrated in *Figure 22* although small corrections from high momentum components in the wavefunction arising from interactions with the

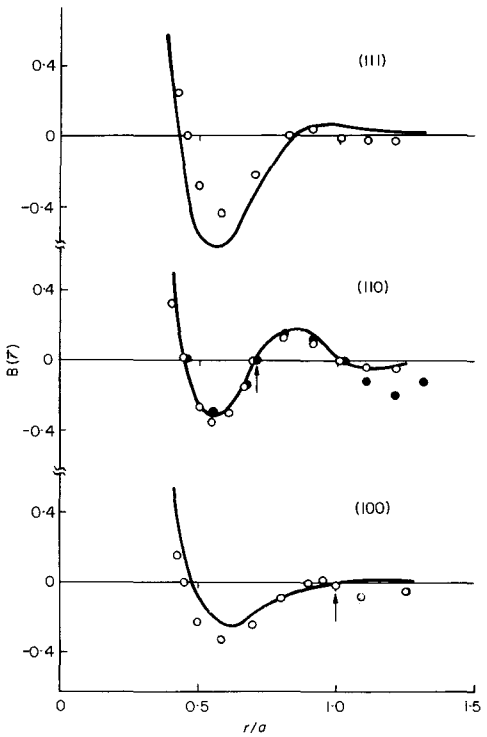

FIG. 21. Reciprocal form factors for silicon. The arrows show the lattice vectors at which the reciprocal form factor must be zero. Distances are given in terms of the lattice constant *a*. The closed circles give experimental data taken from Pattison and Schneider (1978), the open circles give experimental data taken from Reed and Eisenberger (1972) and the solid line is for a Wannier function calculation (Tejedor, 1979).

lattice and from electron–electron correlation are apparent (*see also* Lundqvist and Lydén, 1971, for a detailed discussion of lithium and sodium). The discontinuity in the Fermi surface produces long-range oscillations in the reciprocal form factor (Pattison and Williams, 1976). For simple metals one can use the zero crossings produced by these oscillations to obtain a very accurate measure of the Fermi momentum. With a momentum resolution of only 0.4 a.u. an accuracy in the determination of the Fermi momentum of 0.02 a.u. may be obtained and this has been used by Honda *et al.* (1980) to examine the temperature dependence of the Fermi momentum of aluminium.

5. APPLICATIONS

Diamond and silicon

γ-ray Compton profiles have been measured for diamond and silicon in several crystallographic directions (Reed and Eisenberger, 1972; Pattison *et al.*, 1981) and extensive theoretical studies have been made using a variety of wavefunctions (MacKinnon and Kramer, 1979; Schülke and Kramer, 1979; Tejedor, 1979). Recently Pattison *et al.* (1981) have presented an analysis of the Compton profiles and the

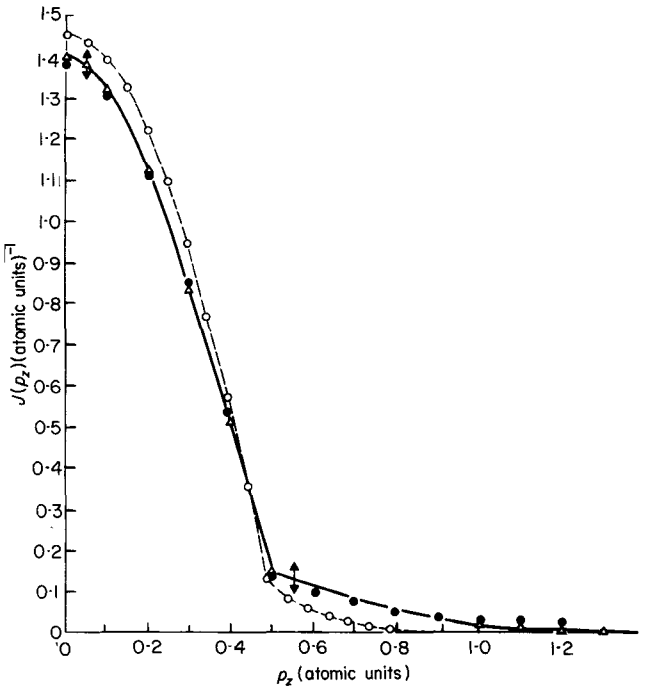

FIG. 22. Compton profiles of sodium. The triangles give the experimental results and the open circles a calculation based on a homogeneous interacting electron gas (Eisenberger *et al.*, 1972). The closed circles are for a calculation which includes the effects of core-orthogonalization (Pandey and Lam, 1973).

reciprocal form factors of these two solids based on their chemical bonds and the interactions between them. Diamond and silicon have the same structure and the same valence electron configuration. However, the valence electrons of silicon are in the L shell while those of diamond are in the M shell. As a result the valence electron wavefunctions of silicon are expanded by a factor of 1.7 relative to diamond (if one simple takes the ratio of the radii of maximum charge density for the valence orbitals) while the silicon lattice is expanded by the slightly smaller factor of 1.52 relative to diamond.

Seth and Ellis (1977) calculated Compton profiles for diamond and silicon in six directions using a discrete variational method and an LCAO Slater basis. Pattison *et al.* (1981) used these results to obtain the reciprocal form factor in each direction and then fitted the results to an expansion in four cubic harmonics to obtain the reciprocal form factor in three dimensions. They also measured the Compton profile of silicon in six directions and treated these results in the same way. For diamond the experimental anisotropy measured by Reed and Eisenberger (1972) is in good agreement with the calculation of Seth and Ellis (1977).

The features in the reciprocal form factor arising from the effects of bonding in the region between 2 and 4 Å are typically about 0.05 times the essentially atomic contribution at the origin. The analysis is therefore facilitated if the results can be plotted as a difference. One approach is to subtract a free atom reciprocal form factor but this is usually so far removed from the reciprocal form factor of the crystal as to be of little use. Subtracting a free atom reciprocal form factor set artificially into the

appropriate hybridization state only improves the situation marginally. Pattison *et al.* (1981) consequently chose to plot differences from the spherically averaged reciprocal form factor. *Figure 23* gives the theoretical anisotropy in the reciprocal form factor for diamond and *Figures 24 and 25* the theoretical and experimental anisotropies for silicon. In these plots the circles give the nearest neighbour distances (diamond 1.54 Å,

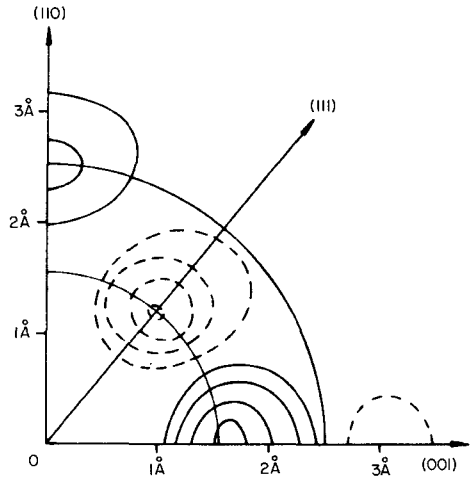

FIG. 23. Anisotropy in the reciprocal form factor for diamond from the calculations of Seth and Ellis (1977). The contours represent intervals of 0.05 electrons. Also shown are the radial distances corresponding to the bond length (1.54 Å) and the second neighbour bond distance (2.52 Å) (Pattison *et al.*, 1981).

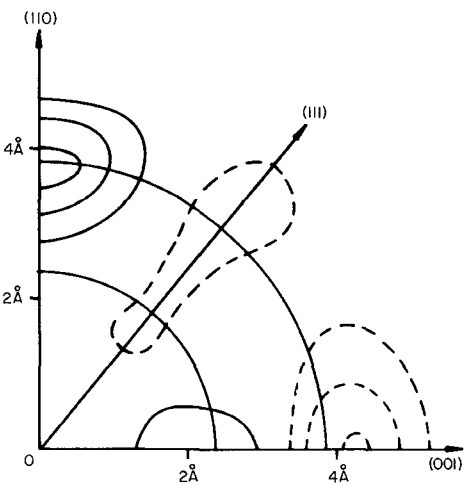

FIG. 24. Theoretical anisotropy in the reciprocal form factor of silicon from the calculations of Seth and Ellis (1977). Contours are at intervals of 0.02 electrons. Also shown are the radial distances corresponding to the bond length (2.35 Å) and the second neighbour bond distance (3.84 Å) (Pattison *et al.*, 1981).

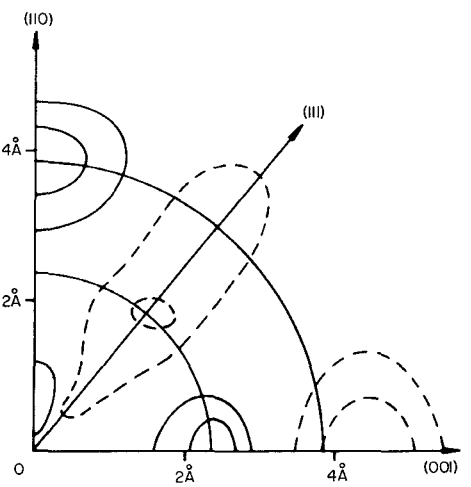

FIG. 25. Experimental anisotropy in the reciprocal form factor for silicon (Pattison *et al.*, 1981). Contour intervals and radial distances are as shown in *Figure 24*.

silicon 2.35 Å) and the second nearest neighbour bond distances (diamond 2.52 Å, silicon 3.84 Å). In both cases the anisotropy has prominent features at these distances. The nearest neighbour atoms are in the ⟨111⟩ direction and the bond orbital may be looked upon as a sum of sp^3 hybrids pointing towards each other as illustrated in *Figure 26*. For such a bond orbital it is shown in Section 4 that there is a negative overlap at a shift corresponding to the bond length. This can be seen in *Figures 23 to 25*, the positive feature in the ⟨001⟩ direction arising from the subtraction of the spherical average. In the ⟨110⟩ direction there is a positive contribution at the second nearest neighbour bond distance. In this direction there is a zig-zag chain of carbon atoms (*Fig. 26*). Using the simple bond orbital description allowance must still be made for the fact that the various bonds are not orthogonal to one another. The overlap with the nearest neighbour bonds makes the resulting orbital more localized along the bond axis. However the overlap with the second nearest neighbour bonds is negative and so to orthogonalize each orbital to its second nearest neighbour requires a positive contribution from these bonds. This gives rise to the positive feature at the second nearest neighbour distance in the ⟨110⟩ direction. Now comparing *Figures 23 and 24* the bond anisotropy in diamond is greater than the second-neighbour anisotropy while the reverse is true for silicon reflecting the fact, noted above, that for silicon, as compared with diamond, the relative expansion of the valence orbitals is greater than the relative expansion of the lattices. Band structure calculations on silicon also demonstrate the importance of second nearest neighbour interactions. Neglecting this and higher order overlaps leads to errors in the band energies of up to 0.5 eV (Kane and Kane, 1978).

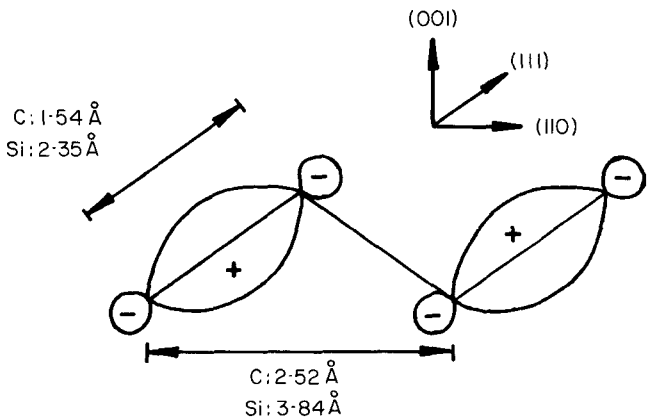

FIG. 26. Schematic diagram of two second neighbour bonds in diamond and silicon.

These results show that Compton profiles are reasonably sensitive to overlaps up to 4 Å. Beyond this distance the overlap effects are of course becoming smaller but, more importantly, in γ-ray experiments the attenuation factor (the Fourier transform of the resolution function) goes rapidly to zero beyond 4 or 5 Å.

This analysis has only dealt with the anisotropy in the reciprocal form factor. If one considers absolute directional measurements, rather than directional differences, Reed and Eisenberger (1972) have shown that for diamond one only obtains close agreement between theory and experiment using wavefunctions near the Hartree–Fock limit. Compton scattering therefore provides a very stringent test of wavefunction quality.

Lithium hydride

Lithium hydride presents an excellent model system for Compton scattering studies of ionic crystals. The lithium and hydrogen ions each have two 1s electrons so that the wavefunction is particularly simple. This discussion is based on the work of Pattison and Weyrich (1979).

The hydrogen-ion wavefunction is very diffuse and is therefore strongly affected by solid state effects involving overlap with neighbouring ions. Using a single Slater 1s orbital to describe the H^- wavefunction, the exponent can be varied in such a way as to minimize the energy of the crystal and a number of calculations have been carried out on clusters of up to thirteen shells of neighbours (Lundqvist, 1954; Hurst, 1959; Grosso *et al.*, 1976). These calculations yield optimized exponents α ranging from 0.72 to 0.84. Kunz (1969), on the other hand, has calculated a numerical wavefunction which gives greater flexibility. The effective exponent then has an average value close to 0.7 but is about 1.15 beyond 3 Å (Pattison and Weyrich, 1979).

For free, isolated ions the wavefunctions of both the Li^+ and the H^- ion are everywhere positive so that their autocorrelation functions are everywhere positive. *Figure 27* shows the spherically averaged reciprocal form factor between 2.5 and 5 Å measured on a powdered sample as well as the theoretically calculated reciprocal form factor for isolated H^- ions with α equal to 0.69 and 1.04. For both values of α the reciprocal form factor is positive but the experimental result has a negative minimum at 3.5 Å. Increasing α narrows the reciprocal form factor but can never reproduce this minimum. The H^- wavefunctions in particular are very diffuse and so the overlap with adjacent ions will be large. To allow for this overlap Pattison and Weyrich orthogonalized the wavefunction on the central hydride ion to its twelve nearest neighbour hydride ions to obtain

$$\Psi(\boldsymbol{r}) = N[\psi(\boldsymbol{r}) + C \sum_i \psi(\boldsymbol{r} - \boldsymbol{r}_i)] \tag{24}$$

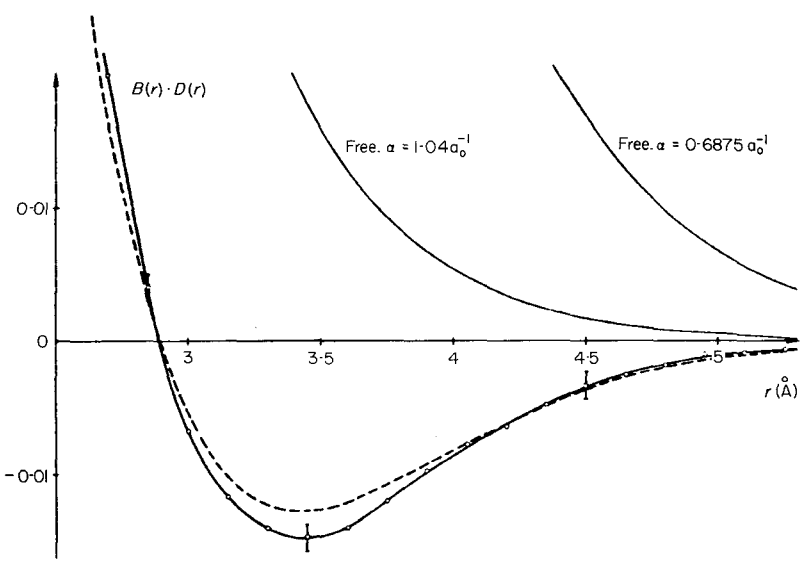

FIG. 27. Comparison between the experimental reciprocal form factor for LiH powder and the hydride cluster model discussed in the text. Results for free hydride ions with $\alpha = 1.04$ and 0.6875 are also shown (Pattison and Weyrich, 1979).

Since the overlap integral between any two hydride ions must be positive the constant C must be negative and the effect of the orthogonalization will be to produce a negative dip in the reciprocal form factor. In the independent particle model the reciprocal form factor must be zero at the lattice translations as shown in Section 4. In the $\langle 110 \rangle$ direction this gives zeros at 2.9 and 5.8 Å so that the negative dip occurs at about 4 Å. By varying the Slater exponent the best fit to the experimental data gave $C = -0.0169$ and $\alpha = 1.04$. This value of α is significantly greater than the values noted above obtained by minimizing the energy of a minimum basis set Slater wavefunction. However, the energy is most sensitive to the wavefunction near the nucleus while the reciprocal form factor is sensitive to the behaviour of the wavefunction at large distances and indeed Kunz's numerical wavefunction has an effective exponent of 1.15 above about 3 Å. As a check on their wavefunction Pattison and Weyrich calculated the diamagnetic susceptibility χ_d which depends on $\langle r^2 \rangle$ and is also sensitive to the outer parts of the wavefunction. They obtained a value of -4.84×10^{-6} c.g.s. units/mole in good agreement with the experimental value of $(-4.60 \pm 0.09) \times 10^{-6}$ c.g.s. units/mole.

Cerium

Of the five phases of cerium the α- and γ phases both have an f.c.c. structure. In spite of the large number of electrons involved (58) this makes the α–γ phase transition ideal for study by Compton scattering. Changes in the observed profile can only depend on changes in the lattice constant or in the occupation of the electronic states. Kornstädt *et al.* (1980) have measured the Compton profiles of both phases and Glötzel and Podloucky (1980) have calculated the Compton profiles using linear muffin-tin orbitals and self-consistent local density potentials.

At room temperature, the transition from γ to α cerium occurs at 0.8 GPa and is accompanied by a 6% decrease in lattice parameter from 5.16 to 4.85 Å. The electronic structure of the outer electrons in cerium is approximately $4f^1 5d^2 6s^1$. Early models of the transition (Koskenmaki and Gschneider, 1978) assumed that the single 4f electron present in the γ-phase is promoted to the 6s conduction band in the collapsed α-phase. Although these models describe the thermodynamics of the transition reasonably well, positron annihilation measurements failed to detect evidence for promotion of the 4f electrons (Gustafson *et al.*, 1969; Gempel *et al.*, 1972).

Experimentally it is observed that the Compton profile of α-cerium is broader than that of γ-cerium and the peak height of the Compton profile is about 0.2 electrons/a.u. less ($\approx 2\%$) than that of the γ-phase Compton profile. Since the α-phase is contracted with respect to the γ-phase this will lead to an expansion of the momentum density of the valence electrons in the α-phase by about 6% even if the electronic structure is otherwise unchanged. The effect on the total Compton profile is to lower $J(0)$ by about 0.1 electrons/a.u. In other words, a simple contraction of the lattice with no change in the valence state explains about half of the observed effect. The question then is, can the remaining difference be accounted for on the basis of a promotion of the 4f electrons to 6s states?

Now for cerium the Compton profile of the free atom 4f electrons ($J(0) = 0.14$) is significantly broader than that of the 6s electrons ($J(0) = 2.1$) (Biggs *et al.*, 1976) so that the promotional model predicts a narrowing of the profile whereas an additional broadening is required. Kornstädt *et al.* (1980) obtain an increase in $J(0)$ if this promotion were to take place in the solid of 0.3 electrons/a.u. whereas a decrease of 0.1 is required. The Compton profile data therefore exclude the promotional model unequivocally. In order to explain the remaining difference of 0.1 electrons/a.u.

Kornstädt *et al.* (1980) calculated the Compton profile using a renormalized free atom model for the s electrons and a tight-binding wavefunction for the d and f electrons. Assuming a $4d^15d^26s^1$ configuration gives good agreement with experiment for γ-phase cerium. The free atom Compton profile for the 5d electrons ($J(0)=0.50$) is also significantly broader than that of the 6s electrons and if 0.6 of an electron is transferred from the 6s to the 5d state a decrease in $J(0)$ of 0.6 electrons/a.u. is predicted in reasonable agreement with the experimental data. However, this model relies on rather crude wavefunctions and so Glötzel and Podloucky (1980) carried out a more extensive calculation. Their angular momentum decomposition of the valence charge gives a transfer of 0.14 electrons from the combined 6(sp) states to the 5d state while the occupation of the 4f state is unchanged. This calculation then gives excellent agreement with the experimental difference curve. These results are summarized in *Table 1*.

TABLE 1. The change in the peak height of the Compton profile for the γ to α phase transition in cerium. The lattice contraction with the promotion of 0.14 electrons from the 6(sp) to the 5d state agrees well with the experimental results. The 4f to 6s does not

	$J(0)_{\alpha-\gamma}$
Experiment	0.20
Lattice contraction	0.10
Atomic $4f^1 \rightarrow 6s^1$	−0.30
Renormalized free atom $6s^{0.6} \rightarrow 5d^{0.6}$	0.06
Band structure $6(sp)^{0.14} \rightarrow 5d^{0.14}$	0.10

The γ-ray Compton profile measurements thus provide strong evidence against the promotional model in which 4f electrons enter the conduction band. Part of the observed change in the electron density arises from the contraction of the lattice; the remainder can be explained in terms of a transfer from the 6(sp) states to the 5d states but only fairly extensive band structure calculations give accurate quantitative agreement between theory and experiment.

Transition metal–aluminium alloys

γ-ray Compton profile measurements have been used to study the charge transfer in FeAl, CoAl and NiAl (Manninen *et al.*, 1981). Measurements were made on powdered samples of each alloy and their constituent metals and it was assumed that in all cases the transfer takes place between the conduction electrons of aluminium and the 3d orbitals of the transition metal. The conduction electron profile of aluminium was obtained by subtracting a free atom core from the experimental data and the 3d profiles of the transition metals were obtained from renormalized free atom calculations. The charge transfer was then varied to obtain the best fit with experiment. In *Table 2* these results are compared with the results of soft X-ray emission measurements (Wenger and Steinemann, 1974; Blau *et al.*, 1979). The trend is similar in all three cases and the difference in the absolute values probably reflects the fact that the charge transfer is not an entirely unambiguous quantity but depends on how it is defined and measured.

TABLE 2. Charge transfer Δn in various transition metal–aluminium alloys. Column (a) gives the results of γ-ray Compton scattering measurements (Manninen *et al.*, 1981) and columns (b) and (c) the results of soft X-ray emission measurements by Wenger and Steinemann (1974) and Blau *et al.* (1979), respectively. Numbers in brackets give standard errors in the last figure

Δn	*a*	*b*	*c*
FeAl	0.40(5)	0.69(5)	0.65
CoAl	0.60(5)	0.88(6)	0.85
NiAl	0.35(5)	0.45(5)	0.60

Magnesium oxide

The electronic structure of MgO is of some interest. Although it is generally assumed that MgO is a purely ionic material in a state $Mg^{2+}O^{2-}$, an isolated O^{2-} ion is not stable so that for this model to be valid the oxygen ions must be stabilized by the crystal field of the lattice. This effect can be simulated by surrounding the O^{2-} ion with a hollow charged sphere known as a Watson sphere. Aikala *et al.* (1982) measured the Compton profile in the [100], [110] and [111] directions and compared their results with nine different theoretical models using a variety of wavefunctions for the oxygen 2p electrons, Watson spheres of various radii as well as an orthogonalized LCAO band wavefunction. Their results support the stabilized ionic model of MgO and enable them to identify those models which give the best agreement with experiment.

Tellurium and selenium

γ-ray Compton profiles have been measured for trigonal selenium and very extensive calculations have been done both for this (Kramer and Schröder, 1977; Krusius, 1977) and for trigonal tellurium (Krusius *et al.*, 1980). Both elements crystallize in the trigonal phase with helical chains packed into an hexagonal lattice. Their calculations lead the authors to conclude that in tellurium the interchain interactions are about three times stronger than in selenium and measurements on tellurium should provide a good test of this prediction. For tellurium a very extensive OPW calculation was carried out using a Slater X-α exchange correction with α equal to 1 and 2/3. The effect of the electron–electron correlation on the momentum density of metals is to smooth out the discontinuity at the Fermi-surface and qualitatively one might therefore expect correlation effects to reduce the oscillations in the reciprocal form factor at large distances. This is observed in the calculated reciprocal form factors for tellurium and the first negative dip at about 3.3 Å is reduced in amplitude by about 10% when α is increased from 2/3 to 1. With careful measurements it should therefore be possible to set an optimum value for the Slater exchange parameter α.

Graphite intercalates

Positron annihilation has been used in a recent series of studies of the electronic structure of graphite intercalates (Pfluger *et al.*, 1980; Cartier *et al.*, 1981. For an extensive review of graphite intercalates *see* Dresselhaus and Dresselhaus, 1981). As noted above, the interpretation of positron annihilation profiles is complicated by the

need to include the positron wavefunction in the theoretical model. However, the repulsion of the positron by positively charged species and its attraction by the electrons furthest removed from the nuclei provides a degree of selectivity as to the electrons which are sampled and this can be used to advantage.

In these studies Li, K, $SbCl_5$ and ICl were intercalated into highly oriented pyrolytic graphite (HOPG) at various degrees of staging. In pure HOPG the positrons are repelled by the atomic cores and annihilate preferentially with the electrons in the π-band. The constituent atomic p_z orbitals point out of the hexagonal plane of the graphite so that the profile should be bimodal parallel to the c-axis, the two peaks corresponding to the projection of the two lobes into this direction. Within the hexagonal plane, on the other hand, the profile should be narrower with a single peak at zero momentum. Making allowances for the fact that the electrons in the σ band also contribute to the profile one can explain the HOPG profiles indicated by the solid lines in *Figures 28 and 29*.

For pure alkali metals the conduction electrons are essentially free. The Compton profile is therefore an inverted parabola cutting off at the Fermi momentum as noted above. *Figures 28 and 29* also show the measured profiles of C_6Li and C_8K (Cartier *et al.*, 1981). Band structure calculations of C_6Li (Holzwarth *et al.*, 1981) indicate that the conduction electron of the lithium is transferred entirely to the graphite π-band leaving a positive anion which repels the positron. In both directions, parallel and perpendicular to the c-axis, the observed profile is consequently very similar to that of pristine HOPG. In C_8K, on the other hand, the observed profile is quite different. In the hexagonal plane the measured profile can be divided into a narrow free electron like

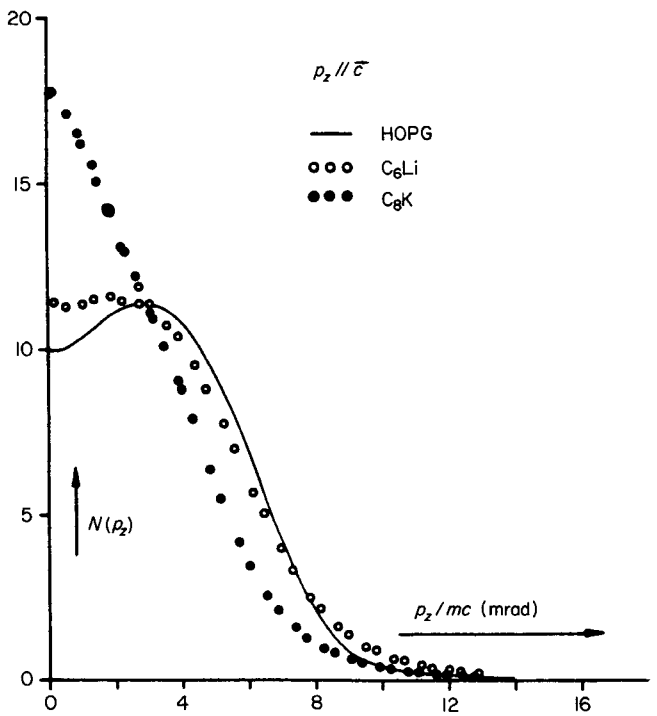

FIG. 28. Positron annihilation profiles of HOPG, C_6Li and C_8K in the direction of the c-axis (Cartier *et al.*, 1981).

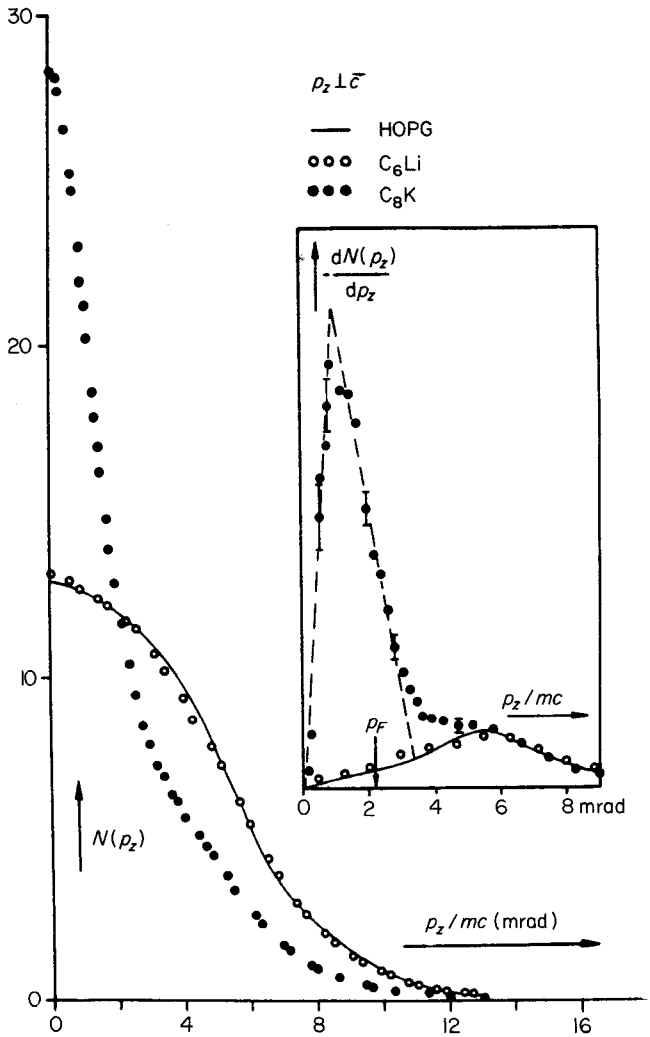

FIG. 29. Positron annihilation profiles of HOPG, C_6Li and C_8K at right angles to the c-axis (Cartier *et al.*, 1981).

contribution superimposed on a broader graphite-like contribution. At right angles to the plane the profile is still narrower than that of HOPG but does not show the distinctive free electron parabola. This directional difference reflects the two-dimensional structure of graphite and the confinement of the positron between the atomic planes. From the discontinuity in their measurement on C_8K in the hexagonal plane the authors obtained a value for the Fermi momentum and hence energy of 1.24 eV which agrees well with the result obtained from photo-emission data (Oelhafen *et al.*, 1980). A free electron gas of potassium conduction electrons at the density found in C_8K would have a Fermi energy of 1.56 eV. Since the number of conduction electrons is proportional to $\varepsilon_F^{1.5}$ the observed Fermi energy corresponds to an electron density of $(1.24/1.56)^{1.5} = 0.7$ electrons/potassium atom or a charge transfer to the graphite π-band of 0.3 electrons/potassium atom. Measurements of the Knight shift in

^{13}C NMR experiments (Conard *et al.*, 1980) give a charge transfer of 0.84 electrons per potassium atom and band structure calculations (Ohno *et al.*, 1979) predict a charge transfer of 0.6 electrons per potassium atom. The relatively low value obtained in the positron annihilation experiments may arise from the assumption of a spherical Fermi surface which could overestimate the number of free electrons present.

In a second study of graphite intercalates (Pfluger *et al.*, 1980) angular correlation profiles were measured in which the intercalates were Li, K, ICl or $SbCl_5$ with a wide range of staging. In the acceptor compounds IBr, ICl and $SbCl_5$ the positron is attracted to and annihilates preferentially with the negatively charged intercalant and the observed profile is then independent of the staging. Furthermore, the observed profiles agree well with theoretical calculations based on the annihilation of a positron with a Cl^- or Br^- ion. In C_nK, the profile depends strongly on the staging approaching that of pure graphite for staging greater than 3 while for the first, second and third stages the results are similar to those discussed above. This supports the contention that for potassium the electronic distortion extends over a distance of approximately two carbon layers.

Transition metal hydrides

For systems containing a large number of different electron states the interpretation of Compton scattering data is difficult. The measured profile is a sum over the individual one-electron profiles, all centred about the same origin, and it is not possible to separate out directly the contributions from each orbital in one measurement. However, this difficulty can sometimes be overcome by carrying out a suitable difference experiment. For example, in a phase transition changes in the electronic structure can be associated with a limited subset of the electrons as in the α–γ phase transition of cerium discussed above. Alternatively, if a light element is added to the host material the change in the electron density arising from the additional electrons can be studied.

An elegant series of measurements have been made in this way on Pd and V hydrides. Lässer and Lengeler (1978) carried out measurements on polycrystalline Pd, V, $PdH_{0.72}$ and $VH_{0.77}$. The sample used to measure the profiles of the pure metals were also used for the hydride measurements to minimize systematic errors arising from effects such as multiple scattering. This is crucial to the success of the experiment as the observed differences are rather small.

The difference profiles (MH_x–M) are shown in *Figures 30 and 31* together with a number of theoretical models in which electrons are transferred between the hydrogen and the conduction band of the metal. In order to construct these models the authors used calculations for the conduction band wavefunctions by Kanhere and Singru (unpublished) for Pd and by Wakoh *et al.* (1976) for vanadium. For the hydrogen atom and hydrogen anion accurate wavefunctions are easily constructed. The d electrons of the transition metals are more localized than the 1s electron of hydrogen and their momentum space distribution is more spread out than that of hydrogen. The full widths at half maximum are 0.51 for atomic hydrogen compared to 1.73 and 1.59 for the atomic d electrons of vanadium and palladium, respectively (Biggs *et al.*, 1976). Transferring electrons to the metal will therefore broaden the difference profile; transferring electrons to the hydrogen atom will make it narrower.

In the anionic model Lässer and Lengeler remove an electron from the conduction band of the metal and use it to create an H^- ion. For both $PdH_{0.72}$ and $VH_{0.77}$ (*Figures 30 and 31*) this gives a difference curve which is much too narrow. In the second 'atomic' model the hydrogen exists as atomic hydrogen and no net charge transfer takes place. These models are now closer to the experimental results but the difference Compton

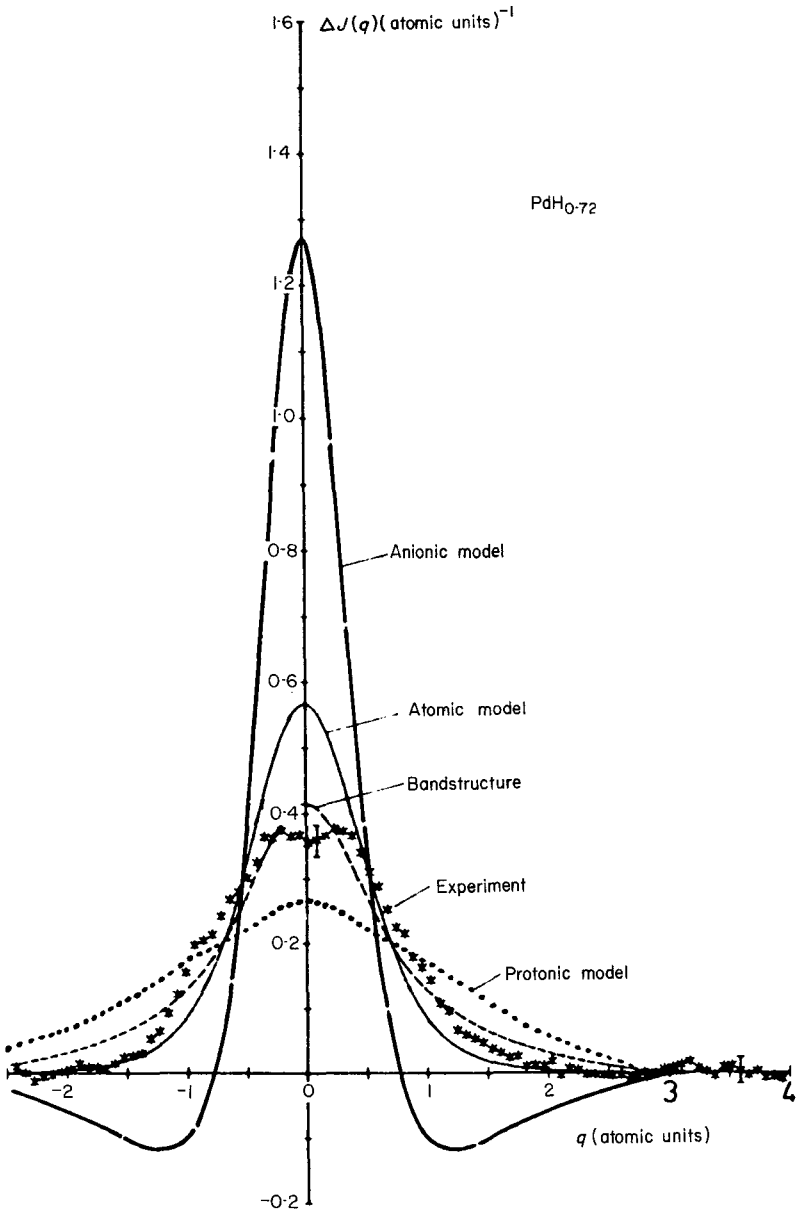

FIG. 30. Difference between the Compton profiles of $PdH_{0.72}$ and Pd compared with four model calculations. Details of the calculations are given in the text (Lässer and Lengeler, 1978).

profiles are still too narrow. In the third 'protonic' model they assume that the hydrogen electron is transferred to the conduction band of the metal but the model profiles are now wider than the observed profiles in both cases. The experimental situation therefore corresponds to a partial transfer of charge from the hydrogen atom to the metal. For $PdH_{0.72}$ a good fit to the experimental data is obtained by taking the

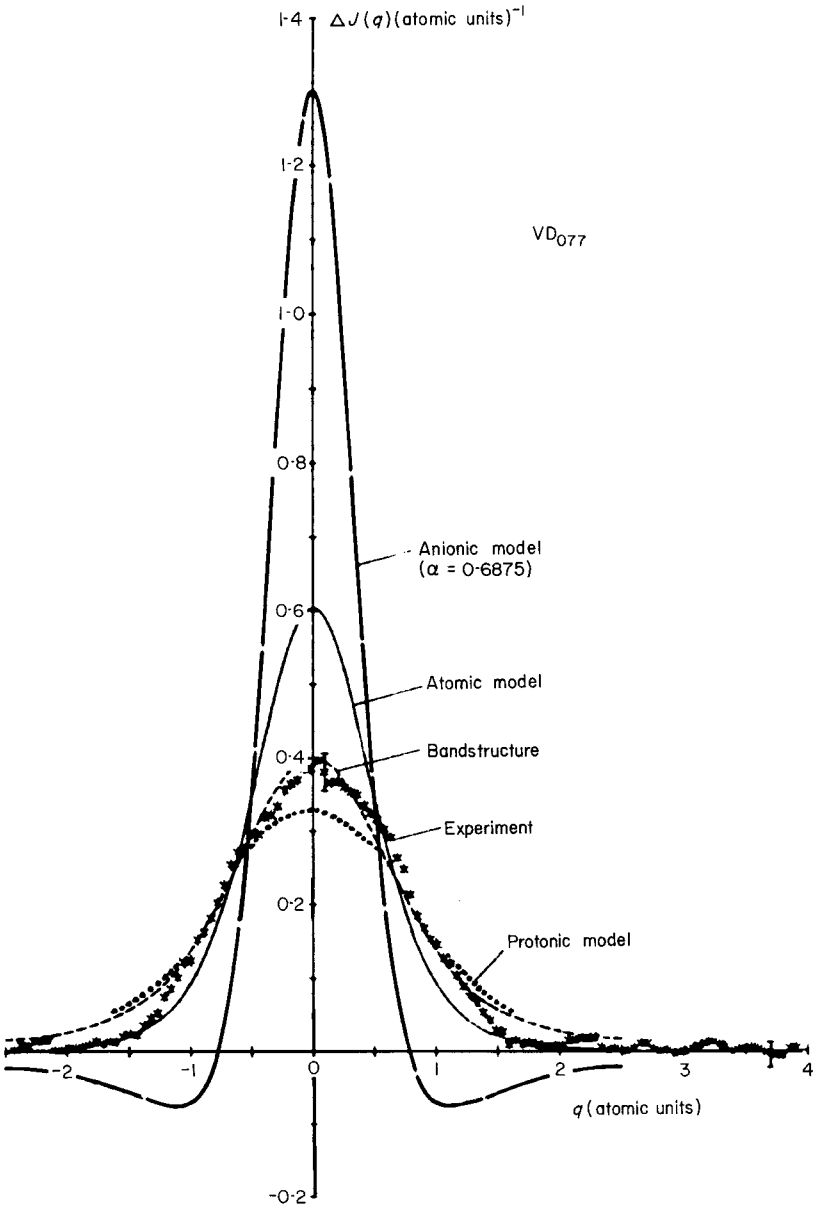

FIG. 31. Difference between the Compton profiles of $VD_{0.77}$ and V compared with four model calculations. Details of the calculations are given in the text (Lässer and Lengeler, 1978).

average of the atomic and the protonic model indicating that half an electron is transferred to the conduction band of the metal. Similarly, in the case of $VH_{0.77}$ the Compton profiles indicate that three-quarters of an electron is transferred to the conduction band of the metal. In a study of $VH_{0.51}$ using positron annihilation Hasegawa *et al.* (1979) obtained similar results.

Clearly, it would be desirable to have wavefunctions calculated specifically for the metal–hydrogen system. For example, the protonic model assumes that the additional electron simply occupies a d-like state in the metal and that neither it nor the protonic charges otherwise distort the wavefunction of the metal. Nevertheless, as the authors point out, the models agree well with the predictions of band structure calculations (Switendick, 1972; Faulkner 1976) and the results of photoemission experiments (Eastman *et al.*, 1971; Antonangeli *et al.*, 1975) and soft X-ray emission spectroscopy (Fukai *et al.*, 1976). The calculations show that the electrons introduced into the lattice by the hydrogen form hydrogen–metal atom bonding hybrids and states which are filled in the pure metal are lowered in energy and shifted below the d states. The Fermi level is moved to higher energies above the d-bands. The newly created hydrogen–palladium bonding states can accommodate 0.5 electrons per hydrogen atom and the hydrogen–vanadium bonding states can accommodate 0.25 electrons per hydrogen atom. The remaining electrons then occupy the d states of the metal.

6. SUMMARY AND FUTURE PROSPECTS

Electron momentum density studies using Compton scattering and the related techniques described in this article are now carried out routinely in a number of laboratories. The processing of experimental data, the calculation of theoretical profiles and the interpretation of the results are well understood. The range of available techniques makes it possible to choose a specific probe to suit the problem at hand. Positron annihilation is best suited for the study of Fermi surfaces for which high resolution (≈ 0.05 a.u.) is required. The use of two-dimensional detectors greatly increases the information content of the data especially in the analysis and interpretation of complicated Fermi surfaces. Furthermore, the shape of the Fermi surface is not affected by the positron wavefunction which otherwise makes quantitative interpretation of the data difficult. (e,2e) scattering provides a powerful probe of the electronic structure of atoms and molecules in the gas phase. The momentum density is observed directly, without integrating over planes and the contributions from different energy states can be measured separately. Gas-phase electron Compton scattering provides very accurate data with excellent resolution (≈ 0.01 a.u.). The viability of carrying out electron Compton scattering from solids with the aid of an electron microscope has now been established and opens up the prospect of measuring the momentum densities of truly microscopic samples and surface layers but is still in the developmental stage. γ-ray Compton scattering is the cheapest and the easiest technique from an experimental point of view but requires rather large samples (≈ 0.05 cm^3) and the resolution is limited (≈ 0.4 a.u.). On the other hand very accurate data (10^8 counts over the profile) can be obtained fairly readily. The development of synchrotron radiation and position sensitive detectors in conjunction with curved crystal analysers has given a new lease of life to X-ray Compton scattering which can now be carried out with good resolution (≈ 0.15 a.u.) at reasonable count rates. However the low incident energies (≈ 10 keV) limit the range of suitable samples to the lighter elements.

In Compton scattering the most important point to bear in mind is that the observed profile is the sum over all the individual electron profiles so that for systems having a large number of distinct electron states it is not easy to interpret the results unless very extensive calculations are available. This difficulty can be overcome to some extent in the study of directional Compton profiles of single crystal samples since the momentum density of the core electrons is spherically symmetric and the anisotropy can be related

to the valence electrons alone. A still more productive approach involves the study of phase transitions or charge transfer, for example, for which changes in the electronic structure can again be related to a limited subset of the electrons.

There are a number of areas in which we anticipate that the application of Compton scattering will provide important information. Graphite intercalates cover a vast range of interesting and important compounds in which molecules may be physically adsorbed on the surfaces of the graphite layers, electrons may be transferred entirely or in part from the intercalant to the π^*-band of the graphite (as in lithium or potassium graphite) or from the graphite π-band to the intercalant (as in IBr or $SbCl_5$ graphite) and this may be done at varying degrees of staging. Other layered compounds such as MoS_2 which takes up hydrogen and is the basis of an important hydro-desulphurization catalyst could also be studied. In this case the amount of hydrogen which can be incorporated in the host is limited so that it may be most suitable for study by positron annihilation. Metallic glasses such as NiNb also take up hydrogen and the study of these systems would provide an interesting extension of the work on palladium and vanadium hydrides discussed in this article.

Metal–ammonia compounds in which lithium, sodium or potassium are incorporated into liquid or solid ammonia have a number of interesting properties. In $Li(NH_4)_3$, for example, it seems probable that the lithium 2s electron is promoted to a 3s state. The lone pair electrons on four of the nitrogen atoms then form a methane-like tetrahedron around the lithium atom inside the charge cloud of the lithium 3s electron. Compton scattering should provide a sensitive test of this model.

Phthalocyanines form crystals in which the molecules are all parallel to one another. Their ability to incorporate metal atoms into their structure makes them important in biology and directional measurements with and without the metal atoms should throw light on the nature of this bonding. Their ultra-stability under electron irradiation make them ideal candidates for study by electron Compton scattering in a microscope.

In recent years there have been a number of developments in the experimental techniques which may contribute significantly to Compton scattering studies (Williams, 1983).

Sakai and Ohno (1976) have observed spin-dependent Compton scattering from magnetized iron using a ^{57}Co source which emits circularly polarized γ-rays. This makes it possible to obtain the momentum density of the unpaired electrons but the experiment is difficult to do and the data so far obtained are of relatively low accuracy. Cooper and Holt (1983) have suggested that similar experiments could be done by capitalizing on the polarization properties of synchrotron radiation. To observe this effect requires circularly polarized radiation while synchrotron radiation is linearly polarized in the orbital plane of the synchrotron. Out of orbital plane the radiation becomes progressively more circularly polarized but, of course, the flux is then decreased. If a suitable compromise between intensity and the degree of circular polarization can be found the study of magnetic materials using Compton scattering will be considerably enhanced.

Under conditions for which dynamical scattering effects are important these may be observed in Compton scattering studies. By adjusting the crystal orientation and the wave-vector of the incident beam it is possible to enhance the scattering from different regions of the unit cell giving Compton scattering a degree of selectivity as to which electrons are sampled. Using X-ray sources dynamical scattering effects have been observed in the Compton profile of silicon in which the relative contributions of the valence and the core electrons were varied significantly (Golovchenko *et al.*, 1981; Schülke, 1981; Schülke *et al.*, 1981). These experiments require perfect crystal samples so that it is unlikely that they will be of wide applicability in X-ray Compton scattering.

In electron Compton scattering the samples are of microscopic dimensions so that perfect crystals are more readily obtained and dynamical scattering effects are easily observed. Williams and Bourdillon (1982) have successfully observed similar effects in the Compton profile of aluminium measured using an electron microscope. The calculation of dynamical scattering effects is by no means trivial but these experiments should provide a useful complement to experiments carried out under kinematic conditions.

A novel approach to γ-ray Compton scattering has been pioneered by MacKenzie (1981, 1982). In these experiments, which he has designated 'active gating γ-ray spectroscopy', a NaI or plastic scintillator provides the sample and the γ-ray source is placed directly between a germanium detector and the sample. A coincidence circuit is then used to ensure that only events in which a γ-ray first scatters from the scintillator and is then registered in the germanium detector are recorded. This eliminates the need for lead shielding and enables one to use a scattering angle of 180°. More importantly, by measuring the energy of the electrons produced in the scintillator it may again be possible to obtain a degree of selectivity as to the electrons which are sampled. MacKenzie (1982) points out that there are many materials which may be used as detectors including liquids, polymers, semi-conductors and inorganic salts.

Finally we should mention the Holy Grail of Compton scattering studies. If one could successfully carry out (e,2e) experiments on solids one would obtain the full four-dimensional (E, k) surface of solids directly. The ability to measure the three-dimensional momentum distribution of oriented samples, with no averaging, and to separate out the contributions from different energies in the bands would be very powerful. Although some of the earliest (e,2e) measurements were carried out on films of amorphous carbon (Camilloni *et al.*, 1979) these were done with low resolution and low count rates and since then no further measurements on solids have been reported. It is not yet clear whether the technical difficulties associated with doing such experiments can be overcome.

ACKNOWLEDGEMENTS

One of us (BGW) would like to thank the Royal Society for the award of a Senior Research Fellowship.

REFERENCES

AIKALA, O., PAAKKARI, T. and MANNINEN, S. (1982). *Acta. Cryst. A*, *38*, 155.

ANDREW, E. R. (1981). *Intl. Rev. Phys. Chem.*, *1*, 195.

ANTONANGELI, F., BALZAROTTI, A., BIANCONI, A. BURATTINI, E. and PERFETTI, P. (1975). *Phys. Lett. A*, *35*, 309.

BARLAS, A. D., RUECKNER, W. H. E. and WELLENSTEIN, H. F. (1978). *J. Phys. B*, *11*, 3381.

BERKO, S. (1977). In *Compton Scattering*, chap. 9 (ed. B. G. Williams), New York: McGraw-Hill.

BERKO, S. and MADER, J. (1975). *App. Phys.*, *5*, 287.

BIGGS, F., MENDELSOHN, L. B. and MANN, J. B. (1976). *Relativistic Orbital and Entire Atom Compton Profiles for the Elements*. Sandia Laboratories, Report Series SAND 75-0636.

BLAU, W., WEISBACH, J., MERZ, G. and KLEINSTUCK, K. (1979). *Phys. Stat. Sol. (b)*, *93*, 713.

BONHAM, R. and WELLENSTEIN, H. F. (1977). In *Compton Scattering* (ed. B. G. Williams), chap. 8, New York: McGraw-Hill.

BONSE, U., SCHRÖDER, W. and SCHÜLKE, W. (1979). *J. Appl. Cryst.*, *12*, 432.

CAMILLONI, R., STEFANI, G., FANTONI, R. and GIARDINI-GUIDONI, A. (1979). *J. Elect. Spect. Rel. Phen.*, *17*, 209.
CARTIER, E., HEINRICH, F., PFLUGER, P. and GÜNTHERODT, H.-J. (1981). *Sol. St. Comm.*, *38*, 985.
COMPTON, A. H. (1922). *Phys. Rev.*, *19*, 267.
COMPTON, A. H. (1923a). *Phys. Rev.*, *21*, 207.
COMPTON, A. H. (1923b). *Phys. Rev.*, *22*, 409.
CONARD, J., ESTRADE, H., LAUGINE, P., FUZELLIER, H., FURDIN, G. and VOSSE, R. (1980). *Physica B*, *99*, 521.
COOPER, M. J. and HOLT, R. (1983) (to be published).
COULSON, C. A. (1941). *Proc. Camb. Phil. Soc.*, *37*, 55 and 74.
COULSON, C. A. and DUNCANSON, W. E. (1941). *Proc. Camb. Phil. Soc.*, *37*, 55.
COULSON, C. A. and MARCH, N. H. (1950). *Proc. Phys. Soc. (London) A*, *63*, 367.
DEBYE, P. J. W. (1923). *Phys. Z.*, *24*, 161. Parts are translated in *Peter Joseph Wilhelm Debye.* Bibliographic Memoirs of Fellows of the Royal Society, *16*, 175 (1970).
DRESSELHAUS, M. S. and DRESSELHAUS, G. (1981). *Adv. Phys.*, *30*, 139.
DONOVAN, B. and MARCH, N. H. (1956). *Proc. Phys. Soc.*, *69*, 1249.
DUBARD, J. L. (1979). *J. Phys. E.*, *12*, 302.
DUMOND, J. W. M. (1929). *Phys. Rev.*, *33*, 643.
DUNCANSON, W. E. (1941). *Proc. Camb. Phil. Soc.*, *37*, 97.
DUNCANSON, W. E. and COULSON, C. A. (1941). *Proc. Camb. Phil. Soc.*, *37*, 406.
DUNCANSON, W. E. and COULSON, C. A. (1942). *Proc. Camb. Phil. Soc.*, *38*, 100.
EASTMAN, D. E., CASHION, J. K. and SWITENDICK, A. C. (1971). *Phys. Rev. Lett.*, *27*, 35.
EDMONDS, D. T. (1982). *Intl. Rev. Phys. Chem.*, *2*, 103.
EGERTON, R. F. (1980). *J. Microscopy*, *118*, 389.
EISENBERGER, P., LAM, L., PLATZMAN, P. M. and SCHMIDT, P. (1972). *Phys. Rev. B*, *6*, 3671.
EPSTEIN, I. R. (1973). *Acc. Chem. Res.*, *6*, 145.
EPSTEIN, I. R. (1975). *International Review of Science, Physical Chemistry*, Series Two, *1*, 107 (eds A. D. Buckingham and C. A. Coulson).
FAULKNER, J. S. (1976). *Phys. Rev. B*, *13*, 2391.
FUJIWARA, K. and SUEOKA, O. (1966). *J. Phys. Soc. Japan*, *21*, 1947.
FUKAI, Y., KAZAMA, S., TANAKA, K. and MATSUMOTO, M. (1976). *Sol. St. Comm.*, *19*, 507.
FURNESS, J. B. and MCCARTHY, I. E. (1973). *J. Phys. B*, *6*, 204.
GEMPEL, R. F., GUSTAFSON, D. R. and WILLENBERG, J. D. (1972). *Phys. Rev. B*, *5*, 2082.
GLÖTZEL, D. and PODLOUCKY, R. (1980). *Physica*, *102*, 348.
GOLOVCHENKO, J. A., KAPLAN, D. R., KINCAID, B., LEVESQUE, R., MEISNER, A., ROBBINS, M. F. and FELSTEINER, J. (1981). *Phys. Rev. Lett.*, *46*, 1454.
GROSSO, G., PASTORI PARRAVICINI, G. and RESTA, R. (1976). *Phys. Stat. Sol. (b)*, *73*, 371.
GUSTAFSON, D. R., MCNUTT, J. D. and ROELLIG, L. O. (1969). *Phys. Rev.*, *183*, 435.
HALONEN, V., EPSTEIN, I. TANNER, A. and WILLIAMS, B. G. (1977). In *Compton Scattering* (ed. B. G. Williams), chap. 4. New York: McGraw-Hill.
HANSEN, N. (1981). *Reconstruction of the Electron Momentum Distribution from a Set of Directional Compton Profiles*, Berlin: Hahn-Meitner Institute, Report Series B342.
HASEGAWA, M., KOIKE, S., HIRABAYASHI, M., ASANO, H. and SUZUKI, T. (1979). *J. Phys. Soc. Japan*, *46*, 481.
HOLZWARTH, N. A. W., RABII, S. and GIRIFALCO, L. A. (1981). *Phys. Rev. B*, *18*, 5190.
HONDA, T., ITOH, F. and SUZUKI, K. (1980). *J. Phys. Soc. Japan*, *48*, 561.
HURST, R. P. (1959). *Phys. Rev.*, *114*, 746.
JONES, W. and THOMAS, J. M. (1979). *Prog. Sol. St. Chem.*, *12*, 101.
KANE, E. O. and KANE, A. B. (1978). *Phys. Rev. B*, *17*, 2691.
KORNSTÄDT, U., LÄSSER, R. and LENGELER, B. (1980). *Phys. Rev. B*, *21*, 1898.
KOSKENMAKI, D. G. and GSCHNEIDER, K. A. (1978). In *Handbook of the Physics and Chemistry of Rare Earths* (eds K. A. Gschneider and L. Eyring), chap. 4. Amsterdam: North-Holland.
KRAMER, P. and SCHRÖDER, W. (1977). *Phys. Rev. Lett.*, *38*, 1227.
KRUSIUS, P. (1977). *J. Phys. C*, *10*, 1875.
KRUSIUS, P., STUBB, T., ISOMAKI, H. and VON BOEHM, J. (1980). *Phys. Rev. B*, *22*, 2955.
KUNZ, A. B. (1969). *Phys. Stat. Sol. (b)*, *36*, 301.

LÄSSER, R. and LENGELER, B. (1978). *Phys. Rev. B, 18*, 637.
LÄSSER, R., LENGELER, B., GSCHNEIDER, K. A., JR. and PALMER, P. (1979). *Phys. Rev. B, 20*, 1390.
LOUPIAS, G. and PETIAU, J. (1980). *J. Physique, 41*, 265.
LOUPIAS, G., PETIAU, J., ISSOLAH, A. and SCHNEIDER, J. (1980). *Phys. Stat. Sol. (b), 102*, 79.
LUNDQVIST, B. I. and LYDÉN, C. (1971). *Phys. Rev. B, 4*, 3360.
LUNDQVIST, S. O. (1954). *Arkiv. for Physik, 8*, 177.
MACKENZIE, I. K. (1981). *Lecture Notes.* Varenna, Italy: Enrico-Fermi International School of Physics.
MACKENZIE, I. K. (1982) (private communication).
MACKINNON, A. and KRAMER, B. (1979). *Sol. St. Comm., 29*, 71.
MANNINEN, S. and PAAKKARI, T. (1978). *Nucl. Inst. Meth., 115*, 1978.
MANNINEN, S., SHARMA, B. K., PAAKKARI, T., RUNDQVIST, S. and RICHARDSON, M. W. (1981). *Phys. Stat. Sol. (b), 107*, 749.
MARCH, N. H. (1954). *Proc. Phys. Soc., 67*, 9.
MENDELSOHN, L. and SMITH, V. H., JR. (1977). In *Compton Scattering* (ed. B. G. Williams), chap. 5. New York: McGraw-Hill.
MEULLER, F. M. (1977). *Phys. Rev. B, 15*, 3039.
RICHARDSON, M. W. (1981). *Phys. Stat. Sol. (b), 107*, 749.
MIJNARENDS, P. E. (1977). *UNFOLD a Fortran IV code for the synthesis of momentum distributions by deconvolution of angular correlation spectra of positron annihilation or Compton line profiles.* Report RCN-217.
MIJNARENDS, P. E. (1979). In *Positrons in Solids* (ed. P. Hautojarvi), chap. 2. Berlin: Springer-Verlag.
MOORE, J. H., TOSSELL, J. A. and COPLAN, M. A. (1982). *Acc. Chem. Res., 15*, 192.
OELHAFEN, P., PFLUGER, P., HAUSER, E. and GÜNTHERODT, H.-J. (1980). *Phys. Rev. Lett., 44*, 197.
OHNO, T., NAKAO, K. and KAMIMURA, H. (1979). *J. Phys. Soc. Japan, 47*, 1125.
PAATERO, P. and HALONEN, V. (1976). *Nucl. Inst. Meth., 135*, 537.
PANDEY, K. C. and LAM, L. (1973). *Phys. Lett. A, 43*, 319.
PATTISON, P., HANSEN, N. K. and SCHNEIDER, J. (1981). *J. Chem. Phys., 59*, 231.
PATTISON, P. and SCHNEIDER, J. R. (1978). *Sol. St. Comm., 28*, 581.
PATTISON, P. and SCHNEIDER, J. R. (1979). *Nucl. Inst. Meth., 158*, 145.
PATTISON, P. and WEYRICH, W. (1979). *J. Phys. Chem. Sol., 40*, 213.
PATTISON, P. and WILLIAMS, B. G. (1976). *Sol. St. Comm., 20*, 585.
PFLUGER, P., ACKERMANN, K.-P., LAPKA, R., SCHUPFER, E., JEKER, R., CARTIER, E. and HEINRICH, F. (1980). *Synth. Metals, 2*, 285.
PLATZMAN, P. and TZOAR, N. (1977). In *Compton Scattering* (ed. B. G. Williams), chap. 2. New York: McGraw-Hill.
PODOLSKY, B. and PAULING, L. (1929). *Phys. Rev., 34*, 109.
RAO, C. N. R., SRINIVASAN, A. and JAGANNATHAN, K. (1981). *Intl. Rev. Phys. Chem., 1*, 45.
REED, W. A. and EISENBERGER, P. (1972). *Phys. Rev. B, 6*, 4596.
SAKAI, N. and OHNO, K. (1976). *Phys. Rev. Lett., 37*, 351.
SCHÜLKE, W. (1977). *Phys. Stat. Sol. (b), 82*, 229.
SCHÜLKE, W. (1981). *Phys. Lett. A, 83*, 451.
SCHÜLKE, W., BONSE, U. and MOURKIS, S. (1981). *Phys. Rev. Lett., 47*, 1209.
SCHÜLKE, W. and KRAMER, B. (1979). *Acta Cryst. A, 35*, 953.
SETH, A. and ELLIS, D. E. (1977). *J. Phys. C, 10*, 181.
SHIZUMA, K., NISHI, M., FUJITA, T. and YOSHIZAWA, Y. (1980). *J. Phys. Soc. Japan, 49*, 2203.
STARK, J. (1909). *Phys. Zeit., 10*, 579.
STARK, J. (1910). *Phys. Zeit., 11*, 179.
STEUWER, R. H. (1975). *The Compton Effect: Turning Point in Physics.* New York: Science History Publications.
STEUWER, R. H. and COOPER, M. J. (1977). In *Compton Scattering* (ed. B. G. Williams), chap. 1. New York: McGraw-Hill.
SWITENDICK, A. C. (1972). *Ber. Bunsenges. Phys. Chem., 76*, 535.

TANNER, A. and EPSTEIN, I. R. (1977). In *Compton Scattering* (ed. B. G. Williams), chap. 7. New York: McGraw-Hill.
TEJEDOR, C. (1979). *Sol. St. Comm.*, *32*, 1303.
WAKOH, S., KUBO, Y. and YAMASHITA, J. J. (1976). *J. Phys. Soc. Japan*, *40*, 1043.
WEIGOLD, E., HOOD, S. T. and TUEBNER, P. J. O. (1973). *Phys. Rev. Lett.*, *30*, 475.
WEISS, R. J., REED, W. A. and PATTISON, P. (1977). In *Compton Scattering* (ed. B. G. Williams), chap. 3. New York: McGraw-Hill.
WELLENSTEIN, H. F., BONHAM, R. A. and ULSH, R. C. (1973). *Phys. Rev. A*, *8*, 304.
WENGER, A. and STEINEMANN, S. (1974). *Helv. Phys. Acta*, *47*, 321.
WEST, R. N. (1980). *J. Phys. Chem.*, *84*, 1286.
WEST, R. N., MAYERS, J. and WALTERS, P. A. (1981). *J. Phys. E*, *14*, 478.
WEYRICH, W., PATTISON, P. and WILLIAMS, B. G. (1979). *Chem. Phys.*, *41*, 271.
WILLIAMS, B. G. (1971). *X-ray Compton Scattering.* University of Cambridge: Thesis for the degree of Doctor of Philosophy.
WILLIAMS, B. G. (1976). *Acta Cryst. A*, *32*, 513.
WILLIAMS, B. G. (1977a) (ed.). *Compton Scattering.* New York: McGraw-Hill.
WILLIAMS, B. G. (1977b). *Phys. Scripta*, *15*, 69.
WILLIAMS, B. G. (1983) (to be published).
WILLIAMS, B. G. and BOURDILLON, A. J. (1982). *J. Phys. C*, *15*, 6881.
WILLIAMS, B. G. and EGERTON, R. F. (1982). *Chem. Phys. Lett.*, *88*, 95.
WILLIAMS, B. G., PARKINSON, G. M., ECKHARDT, C. J., THOMAS, J. M. and SPARROW, T. G. (1981). *Chem. Phys. Lett.*, *78*, 434.
WILLIAMS, B. G., PATTISON, P. and COOPER, M. J. (1974). *Phil. Mag.*, *30*, 307.
WILLIAMS, B. G., VASUDEVAN, S. and RAYMENT, T. (1983). *Proc. Roy. Soc.* (in press).
WONG, T. C., MENDELSOHN, L. B., GROSSMAN, H. and WELLENSTEIN, H. F. (1982). *Phys. Rev. A*, *26*, 181.